A COMPARISON OF PIXEL-BASED, OBJECT-BASED, DEEP LEARNING, AND DATA
FUSION IMAGE CLASSIFICATION APPROACHES IN DELINEATING URBAN TREE
CANOPY IN CITY TERRACE

by

Naman Casas

A Thesis Presented to the
FACULTY OF THE USC DORNSIFE COLLEGE OF LETTERS, ARTS AND SCIENCES
UNIVERSITY OF SOUTHERN CALIFORNIA
In Partial Fulfillment of the
Requirements for the Degree
MASTER OF SCIENCE
(GEOGRAPHIC INFORMATION SCIENCE AND TECHNOLOGY)

May 2024

To my family Enrique Casas, Apurva Uniyal, and Satya Uniyal

Acknowledgements

I would like to thank my advisor Dr. Sedano for guiding me through the intricacies of writing a thesis. Additionally, I would like to thank my committee members Dr. Qi and Dr. Ruddell who were willing to help at every step of the process. Finally, I owe my utmost thanks to Beau MacDonald not only for providing me with a workstation in her lab to finish my thesis but also for being a crucial part of my GIS education throughout my undergraduate and graduate career.

Table of Contents

List of Tables

List of Figures

Abbreviations

CNN   Convolutional neural network

DEM   Digital elevation model

EPA   Environmental Protection Agency

GIS   Geographic information science

LARIAC   Los Angeles Region Imagery Acquisition Consortium

NAIP   National Agricultural Imagery Program

nDSM   Normalized digital surface model

nDTM   Normalized digital terrain model

NDVI   Normalized difference vegetation index

OBIA   Object-based image analysis

PBIA   Pixel-based image analysis

RNN   Recurrent neural network

SAR   Synthetic aperture radar

SVM   Support Vector Machine

TPI   Tree planting initiative

UHI   Urban heat island

UTC   Urban tree canopy

Abstract

Cities have prioritized the utilization of trees and the urban tree canopy (UTC) due to their associated benefits of cooling, atmospheric carbon sequestration, and runoff water interception, among others. However, conditions of inequitable canopy coverage are inherent. Tree planting initiatives, like the City of Los Angeles's Green New Deal, attempt to tackle this inequity through the identification of regions with the greatest lack of, and therefore greatest need for the UTC. Remote sensing and GIS are necessary tools for the city managers to monitor the urban forests and conduct temporal comparisons. Thus, this analysis compared pixel-based, object-based, deep learning, and data fusion image classification approaches in identifying urban tree canopy using very-high resolution multispectral imagery, one-meter resolution LiDAR point clouds, and vector data. An accuracy assessment was conducted to compare each classification method according to type I error, type II error, and classification agreement with ground truth data. A final decision on best classification method is predicated on accuracy as well as methodological complexity, time, and replicability. The data fusion classification provides the result with the best accuracy results across both land cover classes despite its long geoprocessing time. The pixel-based, object-based, and deep learning classifications were unable to produce adequate classification accuracies regardless of improved geoprocessing times. Future analyses may look to automate similar data fusion classifications to produce similarly high classification results at a larger scale.

Chapter 1 Introduction

As global temperatures increase, natural protection against this increased heating effect becomes imperative to maintaining the livability of urban environments. These heating consequences are of great concern in the City of Los Angeles given its infrastructural prioritization of the car as a primary mode of travel and its flat landscape with little existing shade. The city aims to counter the consequences of global warming through sustainable development approaches, including tree planting. In 2019, Los Angeles announced its most recent green legislation, the Los Angeles Green New Deal which calls for the growth and maintenance of a healthy and robust urban tree canopy.

The urban tree canopy (UTC) is the condition of tree canopy cover in a city driven by tree planting. Although the existence of a UTC is not new, its role in urban forestry is still a relatively novel concept. Initially, interest in city tree planting began as a response to the poor living conditions brought on by the industrial revolution, which spurred early planners into leveraging trees as a means of beautification and connectivity through nature (Pincetl et al. 2013). Although this remains a primary goal of the UTC in urban forestry, modern UTC implementation approaches aim to quantify the UTC's natural benefits (i.e. stormwater runoff capture, carbon sequestration, and shade coverage) given new methodological advancements (Pincetl et al. 2013). These analyses, however, rely on the classification and quantification of areal tree canopy change over time to correlate growth and decay trends in the UTC against the growth and decay trends of its provided benefits.

Subsequently, these change-over-time analyses require ample modern and historical classifications of tree canopy which is complicated by limited data availability and processing capabilities due to the technological capabilities of the time. Thus, canopy growth comparison

requires the recontextualization of historic datasets into a tree canopy classification with ample thematic and spatial resolution that matches that of modern data types.

This thesis compared four image classification approaches - pixel-based, object-based, deep learning, and object-based data fusion - in their ability to identify tree canopy at a high spatial resolution. Tree canopy was classified using multi-spectral and light detection and ranging (LiDAR) datasets from 2017, one year before the announcement of the Green New Deal, which builds a base canopy classification with which future practitioners may look to quantify canopy change over time as measure of the Green New Deal's efficacy. Accuracy, analytical complexity, and time were considered in the determination of a best classification approach. With the expected release of very high-resolution LiDAR point cloud coverage over Los Angeles County in 2024, this thesis aimed to identify the optimal image classification type in identifying UTC. Given the Los Angeles Green New Deal's nature as a long-range plan with periodic progress checkpoints, the results of this analysis may be used to collect the necessary information to judge the success of this plan in achieving its tree planting goals. Additionally, given this plan calls for a geographic information science (GIS)-forward approach to UTC management, this thesis looks to identify an ideally reproducible classification workflow in hopes of providing the groundwork for UTC identification across multiple future time steps rather than through a singular comparison of progress.

1.1 Tree Planting in Los Angeles

Given global warming continues to drive increasing global temperatures as world populations increase in global cities, urban greenspaces play an increasingly important role in the climate regulation of cities. Within this context, trees are utilized for their shade benefits and their ability to sequester atmospheric carbon, which is particularly useful in global cities with

high emissions like Los Angeles (Gillespie et al. 2012). Furthermore, urban trees have been associated with positive social benefits including neighborhood beautification and lower perceived levels of stress (Watkins et al. 2017). Although these benefits can be quantified, there is still limited confirmation of the relationship between these benefits and the proliferation of the UTC (Riley and Gardiner 2020). Thus, to better aim the benefits of the UTC at the communities most in need, it is necessary to understand the relationship between UTC growth and the ecosystem service benefits which it provides.

1.1.1 History of Los Angeles's Urban Tree Canopy

Historic analyses of Los Angeles's UTC reveal non-uniform trends to canopy growth across the city's neighborhood council districts. According to Gillespie et al. (2012), total tree density has increased across the Los Angeles Basin and San Fernando Valley whilst density decreased in Hollywood since 1920. That said, canopy density increased in a uniform fashion across private land whilst canopy density did not follow the same uniform pattern of growth on public land (Gillespie et al. 2012). This research exemplifies that time-series analysis of tree density and cover to be a primary methodological typology in urban forestry, however, it also reveals major limitations to tree identification in dense conditions. Furthermore, this research marked the beginning of tree planting which targeted vacancies in the public right-of-way.

1.1.2 Los Angeles's Current Tree Planting Approach

Notable modern investment in robust tree planting initiatives (TPIs) in the City of Los Angeles began in 2006 with the announcement of the City of Los Angeles Million Trees initiative, which responded to the history of stagnant tree growth on public land in comparison to private land noted above through a one-million tree planting commitment (McPherson et al. 2008). Said initiative determined that only about 20% of the potential benefits incurred by the

3

proposed planting contributed to natural benefits like carbon sequestration and stormwater runoff, however, this would still result in approximately $1.95 billion in savings by the year 2040 (McPherson et al. 2008). Whilst the Million Trees initiative proposed marked monetary benefits from tree planting, it alternately revealed gaps in the city's GIS infrastructure including a lack of a county-wide tree inventory, which tracks tree growth and health characteristics, and a lack of a central data hub.

Mayor Eric Garcetti revealed Los Angeles's Green New Deal in 2019 which features Los Angeles's next milestone tree planting commitments. The commitment not only calls for the citywide planting of 90,000 new trees but a 50% canopy area increase in neighborhoods of greatest need with baseline growth of 20% across the city. The plan's greatest potential contribution to the academic meta on urban tree canopy, however, is its prioritization of tree protection programs which leverage state funding to preserve older trees which have grown a mature canopy. This is supplemented by the desired development of 'Adopt-A-Canopy' programs which call for homeowners to grow young saplings on their property. By planting trees in safe locations outside of the public right-of-way, tree mortality fueled by vandalism and motor accidents will decrease ultimately contributing to the growth of a more mature and resilient future canopy. That said, this complicates the management process given tree maintenance after planting is the responsibility of the resident meaning the success of these programs are reliant on both homeowner capability and interest in fostering tree growth.

1.1.3 Los Angeles Canopy Management

Since the announcement of the Green New Deal, the City of Los Angeles has contracted private tree management company Davey Trees in the creation of a citywide tree inventory which captures tree size, species, health, and management characteristics, responding to the

informational gaps of Los Angeles's past tree management approaches. Furthermore, the Los Angeles Region Imagery Acquisition Consortium (LARIAC) has announced their new data product list expected to release summer 2024, which includes very-high resolution orthoimagery products standard in tree canopy remote sensing analyses.

This marks a notable modern advancement in the GIS approach toward urban forestry in the City of Los Angeles. The improved data products from LARIAC are directly applicable in the derivation of terrain and surface features in urban settings which could allow researchers to identify the UTC through the volatile surface conditions of tree canopies. The city's contract with Davey Trees also marks its transition into a more robust street tree management approach in which canopy health and growth conditions can be identified at the individual tree level rather than approximating canopy health through a calculation of canopy change over time. Despite these technological advances in the city's GIS urban forestry infrastructure, historical data sources used in past urban forestry research are still limited by the technology of their time rendering their use in modern urban forestry limited due to non-similar temporal, spatial, and thematic resolutions. However, assessments of canopy development, like change over time analyses which attempt to correlate canopy growth and decay against socioeconomic indicators of wealth, require historical data to be in like resolutions to maximize the actionability of these results. In response, this thesis compared the effectiveness of four different image classification methodologies in classifying the UTC at an ample and actionable resolution with which practitioners can develop future tree canopy growth methodologies.

1.2 Study Area

Located due east of downtown Los Angeles, as seen in Figure 1, the unincorporated neighborhood City Terrace is an epicenter of Los Angeles's urban forestry efforts. The

neighborhood boasts a 95% Latino population, approximately a third of which are either elders or children (Urban Trees Initiative 2023). Additionally, given 70% of households fall far below the federal poverty level, much of which can be correlated with historic redlining practices, the neighborhood's population is especially vulnerable to the socioeconomic impacts of the UTC. As a result of the robust industrial presence in the neighborhood, observed particulate matter concentrations are up to 90% higher than the average of other neighborhoods in California (World Health Organization 2021). Given these conditions, UTC development in City Terrace is notably limited making the neighborhood an area of interest for TPIs. The University of Southern California's Urban Trees Initiative research project, in partnership with the City of Los Angeles, has identified City Terrace as a target neighborhood for tree planting efforts which have spawned out of the Green New Deal. Thus, the study area used for analysis was the geographic region defined by the City Terrace neighborhood of East Los Angeles.

Figure 1. City Terrace study area boundary

Due to its large area of residential zoning, the City Terrace study area has high potential

for UTC growth. As seen in Figure 2, City Terrace is comprised of primarily residential zoning.

Commercial zoning is primarily situated around larger, through-traffic streets which are expected

to have higher densities of street tree cover given their role as beautification in commercial

centers. The northern-most portion of the study area is dedicated nearly exclusively to industrial

zoning; however, this area is bordered by residential zoning indicating potential for either high or

low tree canopy coverage. Given the proximity of residential zoning to industrial zoning in this

area, ample tree canopy coverage is important as a counter to the consequences of the industrial

presence. Blue zones in Figure 2 are indicated as government zoning, however, comparison

against ground truth imagery reveals these zones to be primarily local parks. Thus, the City Terrace study area has high potential for future tree canopy growth, however, current tree canopy development may be limited by alternate socioeconomic factors including neighborhood income and social standing.
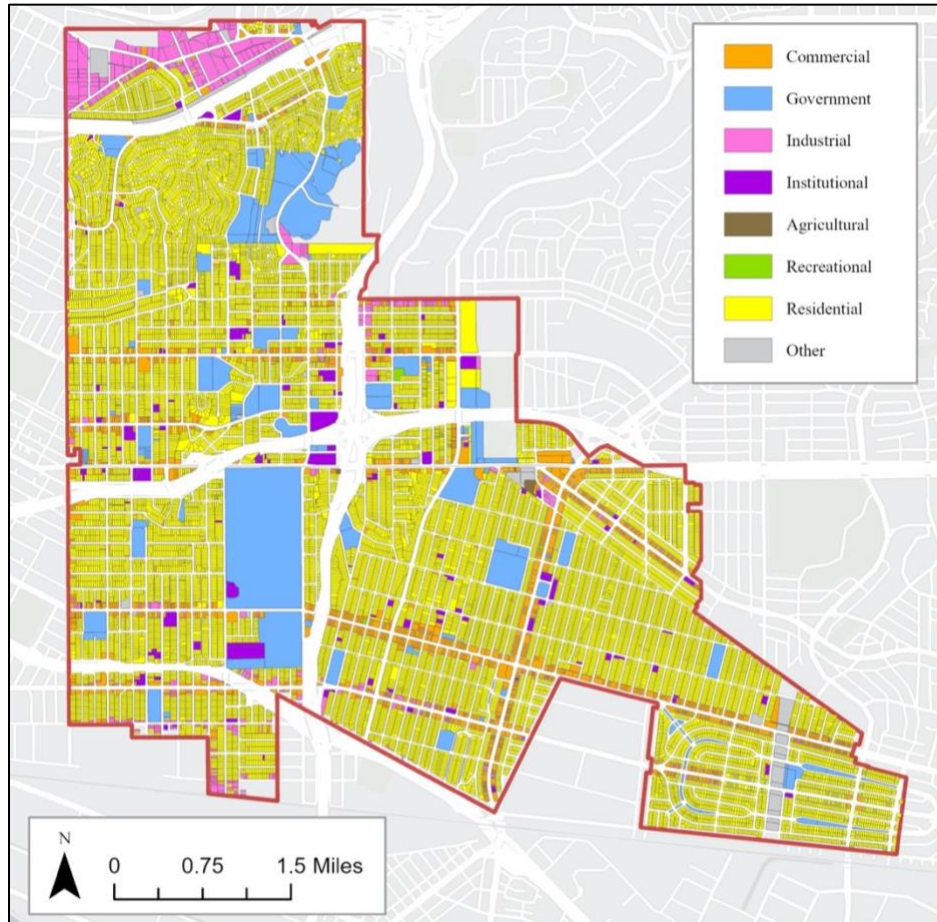
Figure 2. City Terrace land use zoning

1.3 Methodological Overview

This thesis compared pixel-based image analysis (PBIA), object-based image analysis (OBIA), deep learning, and data fusion image classification in their ability to accurately identify and quantify UTC cover using LiDAR point cloud data and 4-band satellite imagery. The PBIA,

conducted in ArcGIS Pro, applied 700 training data pixels to an SVM classifier to classify 4-band satellite imagery into first a seven-class land cover schema which was subsequently derived into 'tree' and 'not tree' classes. The OBIA, similarly conducted in ArcGIS Pro, applied 700 training data polygons to an SVM classifier to classify image objects pre-segmented from 3-band satellite imagery into a seven-class land cover schema which was again reclassified into 'tree' and 'not tree' classes. Using ArcGIS Pro's deep learning extension library, the 'tree segmentation' deep learning algorithm derived from the DeepForest model was used to identify tree canopy objects in 3-band imagery. Finally, in Trimble's eCognition, 4-band imagery derivatives and LiDAR surface raster derivatives were used to segment and reclassify image objects derived from LiDAR point cloud data into a 'tree' and 'not tree' classification of land cover. Finally, each of these classification results were accuracy assessed via confusion matrix building on a stratified random sampling method.

1.4 Thesis Overview

Chapter 1 has discussed the history of Los Angeles's TPI approach, the analysis study area, and overall project goals. Chapter 2 discusses the consequences of urbanization, the role that trees play in managing these consequences, Los Angeles's tree planting approach, and the use of remote sensing in managing this approach. Chapter 3 outlines analysis design, specifically the different remote sensing classification approaches and how they were compared via pixel-based accuracy assessment. Chapter 4 provides the results of this analysis whilst chapter 5 discusses the implications of these results, specifically by deciding which classification approach is best and how future analyses may look to improve upon each classification.

Chapter 2 Related Work

As awareness of the detriments of urbanization increase, the use of trees in improving the urban condition is seen as an important tool in both natural and social ecosystem management. Given the expected heating impacts of climate change as well as its exacerbation of drought conditions in Los Angeles, a sustainable approach toward climate management is necessary. Los Angeles's prioritization of cars through robust street and freeway systems means the city land cover is comprised of primarily impervious surfaces which exacerbate the heat island effect, a condition in which the sun's rays are trapped in these surfaces leading to increased temperatures. As populations are expected to grow, the number of people who are subjected to the consequences will only increase. Furthermore, given the nature of urban trees as a social amenity, socioeconomic and demographic biases drive canopy growth leading to an inequitable distribution of its benefits. This chapter discusses how the UTC can be leveraged as a means of sustainable development and how current methodological advancements in the monitoring of the UTC can be used to plan more equitable tree planting.

2.1 Consequences of Urbanization

The rapid and extensive urbanization fostered in urban cores, like Los Angeles, is understood to produce numerous detriments to the ecosystem health of cities. The three fronts of urbanization's impact on the natural environment of urban cores include impacts on water systems, air quality, and urban heating. A primary facet of urbanization's consequences to urban water systems is a growing concern with mass water storage and their supply chains (Lundqvist, Appasamy, and Nelliyat 2003). Although current remedies include outsourcing water supply

from regional agricultural reservoirs, these become both financially and logistically implausible as population thresholds are approached (Srinivasan et al. 2013).

Research into urban heat islands (UHI), a phenomenon in which heat is trapped and amplified in the hardscape which defines urban environments, reveal marked increases in average temperatures, incidence of extreme temperature pockets, and the disparity between average temperatures of urban environments and their rural counterparts (Xiong et al. 2012). Figure 3, from the United States Environmental Protection Agency (EPA), adds context to these findings by revealing how surface and air temperatures compare per land cover type, revealing the severity of the built environment's heat trapping effects. This figure indicates that as neighborhood typology transitions from rural to the urban core the disparity between day and night air temperatures decrease given the urban hardscape traps heat longer.
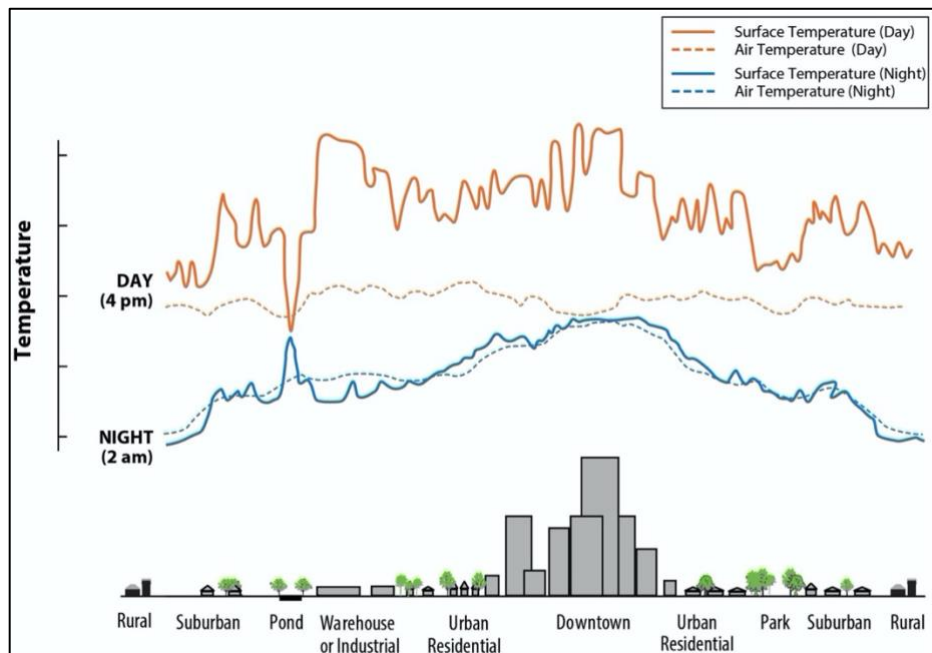
Figure 3. Night and daytime difference in retained surface and air temperatures per locale. Figure by US Environmental Protection Agency

Finally, concerns with urbanization's impact to air quality are of particular interest, especially in Los Angeles which has boasted some of the highest global emission through the middle of the 20th century (Hassler et al. 2016). According to the World Health Organization, high rates of PM 2.5 emissions are a primary contributor to high mortality rates worldwide. Furthermore, research indicates that conditions of increased PM 2.5 are correlated with high population densities especially in areas with inherently dusty emissions, both of which are notable characteristics of Los Angeles (Han, Zhou, and Li 2016).

The natural consequences of urbanization are only expected to amplify given future population growth trends and their correlation with global climate change. The United Nations expects 70% of the global population to inhabit urban cores by 2050, a 20% increase from current population levels. Thus, global water shortages are expected to affect up to 3.1 billion people globally because of seasonal shortages incurred by increasingly severe and frequent drought conditions (McDonald et al. 2011). Additionally, given the higher heat fluxes of the impervious surfaces of urban cores paired with increased urban build-up as a response to increasing population demands, nighttime UHI heating thresholds are expected to increase by up to 30 degrees Fahrenheit by 2050 given increasing global temperatures (Wang et al. 2016). Thus, it is important for the legislative powers which control the regulation of urban systems to implement changes which limit the ecosystem impacts of urbanization.

2.2 Urban Tree Canopy

The UTC is the condition of canopy cover created through tree planting in urban conditions. Although historically used as a means of city beautification aimed at fostering community, modern iterations of tree canopy development prioritize the use of the tree canopy as

means of sustainable development. Canopy benefits in Los Angeles produce monetary, health, and ecological benefits, however, this relies on the maintenance of a mature and healthy canopy. The ecosystem and health benefits of the urban canopy range from storm water management and filtration, temperature mitigation through shade cover, air quality improvement through the filtration of atmospheric particulates, and mitigation of perceived stress. Although this is universally desired, equitable tree canopy growth is inhibited due to social and demographic drivers of social stability including minority status and median household income.

2.2.1 Ecosystem and Health Benefits

Modeling of the environmental benefits of the UTC point to potential monetary savings, however, this success is reliant on a mature tree canopy. Common applications of greenspace in urban centers include public parks, community gardens, hiking trails, water systems, and conservation areas, however, understanding and application of the UTC's role in green urban infrastructure is still novel (Roy, Byrne, and Pickering 2012). As the body of academic research on the benefits provided by the UTC has expanded, however, its role and importance in providing both ecosystem and health benefits has become increasingly evident. Xiao and McPherson (2002) finds that the existing UTC in Santa Monica, California captures 1.6% of yearly precipitation which translates to approximately $111,000 in runoff stormwater treatment and flood control cost savings. This research points to a strong disparity in savings dependent on tree size in which large, mature trees intercepted up to 40% more rainfall in comparison to smaller trees. This points to the importance of tree size and maturity in relation to the benefits of the UTC aside from the larger area of shade they may cast.

Although modeling on the cooling effects of the UTC indicates a direct correlation, the proliferation of these benefits relies on the three-dimensional structure of the canopy. In a model-

based comparison of the temperature cooling benefits of urban trees and grass lawns, Wang et al. (2016) reveals cooling impacts of up to 5 degrees Celsius at peak times, however, also points to a disparity in both the structure of and cost of achieving these benefits. Firstly, lawns induce cooling secondarily by reducing the heat which contributes to vaporization during green evapotranspiration whilst trees produce more direct shade impacts by intercepting solar radiation from reaching and reflecting off the ground (Wang et al. 2016). Furthermore, the cooling impact of trees can be further compounded by increasing canopy density and understory presence in the third dimension whilst scaling of the shade benefits of lawns is limited to the second dimension. Figure 4 illustrates common tree forms and their respective shadow. Round, vertical-oval, and horizontal oval tree canopies project a more substantial shadow on the ground plane while pyramidal and columnar produce narrower features whose shadow is elongated as the aspect between the sun and the tree decreases.
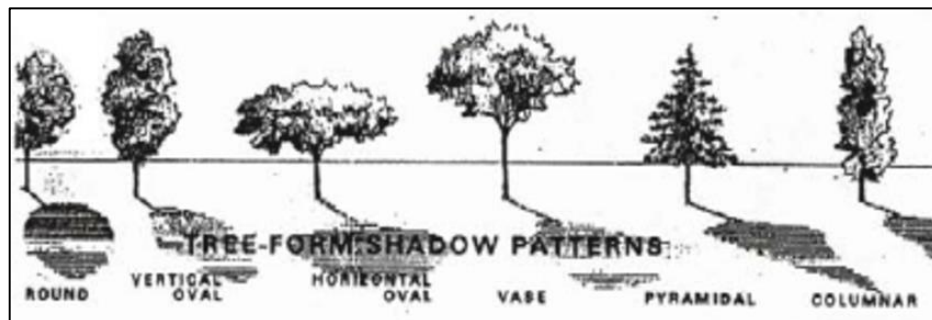
Figure 4. Tree-form shadow pattern diagram. Image from Shahidan and Jones (2008)

Most importantly, urban trees require less water to grow and maintain given their drip irrigation watering systems have more control over water waste relative to traditional lawn sprinklers (Wang et al. 2016). Although the benefits achieved by supplementing the UTC with other green climate mediators, like the lawn, may be implied, model-based life cycle assessments

of their relationship are limited due to complications variable collinearity (Spatari, Yu, and Montalto 2011).

2.2.2 Inequity in the UTC

Although the benefits of the UTC are both observable and quantifiable, variable correlation in the socioeconomic drivers of canopy distribution reveal inequity in the distribution of the UTC in urban regions. Tree canopy cover exhibits a positive relationship with population density in which canopy cover and accessibility increases in more populous regions. Although this expected, this information can be used as normalization in analyses which aim to identify the socioeconomic drivers of canopy growth. For example, Zhuang, Xie, and Yu (2023) identifies a starkly positive relationship between UTC and housing prices in Guangzhou, China pointing to an economic bias in canopy distribution. This research also reveals a positive relationship between UTC and neighborhood age, suggesting stagnant canopy growth in older neighborhoods which has yet to be addressed with current planting initiatives. Additionally, Watkins et al. (2017) applies a statistical regression to correlate the presence of tree canopy with various demographic and socioeconomic factors of stability. This analysis finds higher incidence of planting initiatives in communities with higher percentages of African American and Hispanic residents pointing to a racial bias in accessibility. Furthermore, the neighborhoods with both low median income and high ethnic minority composition had the lowest incidence of TPIs pointing to a compounding of these negative biases (Zhuang, Xie, and Yu 2023). Thus, the socioeconomic drivers of inequitable canopy distribution must be understood together rather than as independent influences.

2.3 Urban Tree Planting Approaches

To counter the negative effects of urbanization and their inequitable distribution across the spatial domain, many cities implement TPIs as a commitment to leverage trees as a counter benefit. The United States' investment in these planting programs began in the mid-20th century as a response to mass Elm tree loss due to Dutch elm disease (Eisenman et al. 2021). The occurrence of these initiatives has since grown including a seven time increase academic publications focused on the matter in the last decade (Eisenman et al. 2021). Most TPIs function at small scales given the amount of public investment required, however, both New York City and the City of Los Angeles have proven successful in implementing larger scale programs. This, however, is reliant on the fact that these larger cities are better equipped to coordinate efforts between public, private, and non-profit constituents in maintaining the commitments of planting initiatives (Roman et al. 2015). TPIs also act as important political leverage for both lobbying and campaign efforts which in smaller cities with less non-profit and private leaderships can prove detrimental to their lasting success (Pincetl et al. 2013). Thus, modern planting initiatives must take a multi-faceted approach toward urban forestry in which the governing bodies that control them take both a coordinated, community focused approach toward canopy management. In this instance, non-profit organizations involved in community tree planting may look to employ private, neighborhood-level TPIs which properly address the ethnic biases of their community whilst city legislators would bolster these efforts with citywide, public planting commitments aimed at catalyzing economic development through their scope and scale.

2.4 Remote Sensing in Urban Forestry

As the technical capabilities of modern remote sensing technologies have improved, urban forest management constituents have adopted the use of satellite imagery in the

identification and management of the UTC. Through the development of remotely sensed data types, like the ability to capture hyperspectral data in high resolution and the use of passive remote sensing to collect 3D point representations of the earth's surface, remote sensing urban tree canopy management methodologies have improved in their ability to accurately quantify the area and location of UTC cover. Standard techniques include the reclassification of high-resolution satellite imagery via pixel- or object-based image analyses as well as the transformation of four-band imagery into representations of vegetation health; However, modern methodological advancements in the application of remote sensing techniques allow for the combination of data types and identification techniques into a single 'data fusion' workflow which expands on the temporal and spatial limitations of traditional approaches.

2.4.1 Data types

Despite the growing public availability of remotely sensed data, the longer geoprocessing times associated with larger remotely sensed datasets limit their widespread usability. Medium resolution imagery from MODIS and Landsat are most often employed in time series-based change monitoring and detection analyses, however, their resolution causes pixel mixing which confidence in the accuracy of their results (Shojanoori and Shafri 2016). Furthermore, this imagery has long collection cycles which limits their use in time series analyses given less data is available per time step. High or very-high resolution satellite imagery is preferred in urban forestry applications given its clear image picture allowing for high-accuracy object identification (Agarwal et al. 2013). QuickBird, IKONOS, and WorldView-2 satellites provide the most popular high-resolution imagery given their inclusion of multispectral bands which can be used to better identify vegetation in complex urban scenes (Ouma and Tateishi 2008).

Limitations caused by the large file size and high cost of hyperspectral imagery limits its widespread application which has lead practitioners in the direction of active sensing options like synthetic aperture radar (SAR) and LiDAR to develop techniques on capturing 3D tree shapes. Most commonly, SAR data is used in natural forest health evaluation given the SAR can penetrate through the ground surface to study tree root health. Alternatively, like in Sung (2012), LiDAR data is used in calculating tree heights and canopy shape via the subtraction of ground return LiDAR values from canopy return values which identifies trees in areas of high difference values between first and last return LiDAR points. This calculation, however, is limited in urban scenes due to the presence of rooftops which are confused with canopy. Rather, in urban settings LiDAR data is used supplementarily to identify structural characteristics like 3D canopy shape and height whilst hyperspectral imagery is used more traditionally to identify vegetation characteristics like species and health (Zhong et al. 2022).

2.4.2 Techniques

Given the dense spatial condition of objects in urban scenes, the identification of tree and other object features in satellite imagery is differentiated between traditional pixel-based approaches and newer OBIA methods. PBIA requires the creation of training datasets in which pixels in the image scene are classified into new land cover classes. This identification type only considers the information hosted in each image pixel in its identification decision, which leads to easier and faster geoprocessing, however, is limited by issues of image speckling and pixel mixing which cause error in the final classification (Shojanoori and Shafri 2016). Alternatively, OBIA models leverage the information from neighboring pixels, including color, shape, and texture, in their decision of classification results (Shojanoori and Shafri 2016).

Although OBIAs may be expected to produce better classification results given their consideration of both spatial and spectral characteristics, final classification accuracies inevitably vary depending on the characteristics of a proposed study area resulting in unique application conditions. In a comparison of PBIA and OBIA techniques, Sibaruddin et al. (2018) finds that OBIA produced final classifications up to 21% more accurate than their pixel-based alternatives. That said, two of the five tested classification scenarios returned OBIA results only about one percent more accurate than their pixel-based counterparts. In fact, although they produce inherently less accurate results, PBIAs are useful in the case of big data given ease and speed of geoprocessing (Sibaruddin et al. 2018). Ultimately, their application in forestry is limited to natural forest detection given the presence of objects in the scene, like buildings, which may create classification confusion. Thus, OBIAs are the standard classification approach in urban forestry given their consideration of object shape characteristics which can be trained to differentiate canopy from conflating objects like building rooftops.

To avoid the manual processes required by standard PBIA and OBIA approaches, practitioners employ deep learning classification models built on neural networks for image object classification. Neural networks are a means of artificial intelligence which automate the processing of input data according to numerous processing layers into a final output (Ma 2019). In the case of their use in remote sensing, deep learning algorithms are incorporated in the training, segmentation, and classification steps of image classification methodologies to eliminate the time dedicated to these manual processes (Ma 2019). The convolutional neural network (CNN), the most popular deep learning image classification model, is used to process singular data inputs according to multiple output arrays and is thus best suited for the classification of multispectral imagery (LeCun, Bengio, and Hinton 2015). In contrast, recurrent

neural networks (RNN) are applied when processing input and output data of varying sequential lengths and are thus best suited in analyses with sequential inputs (Ma 2019). Thus, derivative RNN models are useful in multi-step classification processes whilst CNNs best service one step processes which classify imagery with training data.

2.4.3 Applications

Despite the prevalent use of both active and passive sensor types in capturing remotely sensed imagery, larger methodological applications of remote sensing in urban forestry are primarily focused on location identification, species identification, and structural detection. Tree location detection methodologies are a standard application of remote sensed imagery in urban forestry given they can be conducted using both manual visual-interpretation and computer-driven image classification techniques. Visual interpretation is most useful in supplementary land cover classification given the inherent human error involved. Unsupervised PBIA methods provide a marginal increase in analytical difficulty given these do not require the creation of training datasets, however, these often result in inaccurate, pixelated results in urban conditions due to this lack of image training (Shojanoori and Shafri 2016). In response, supervised PBIA models, like maximum likelihood, minimum distance, and the SVM, are employed, however, still struggle with image pixelization given the spectral variability of urban settings (Yu, Chen, and Chang 2006). Thus, researchers alike prefer object-based models, like the Artificial Neural Network which rely on fuzzy classification logic, given their improved classification results in urban settings (Liu and Xiao 2010). Not only do these techniques improve classification accuracy but allow for the extraction of additional tree characteristic information.

Urban tree canopy detection in urban forestry remote sensing improves on the techniques employed to improve tree counting accuracies. Unlike individual tree counting approaches, tree

canopy detection research leverages an array of spectral information instead relying on physical

object characteristics in the image, like texture and shape, as classification determinants. Thus,

OBIA is preferred over PBIA approaches, however, is instead applied on high-contrast imagery

and imagery derivatives, like the Normalized Difference Vegetation Index (NDVI), which better

differentiate shapes in an image (Liu et al. 2004). Figure 5 is the calculation of the standard

deviation of LiDAR point elevation which reveals tree canopy in a stark white contrast given the

variable three-dimensional structure of tree canopy. This contrast improves object-based imagery

classifications.

Figure 5. Standard deviation of LiDAR point cloud elevation. Image from O'Neil-Dunne et al.
(2013)

Additionally, Yao and Wei (2013) and like researchers reveal the benefit of LiDAR in

revealing 3D structure in remote sensing analyses. Given LiDAR can penetrate and detect tree

canopy in the z-dimension, this data is integrated with 2D classification products to improve

overall classification accuracies beyond that which can be achieved with exclusively LiDAR or

2D imagery classification techniques. However, the use of LiDAR in tree canopy detection scales in difficulty in the transition from natural to urban forests given the increase in structural and spectral complexity of urban scenes. In fact, Yao and Wei (2013) find that misclassification of tree canopy in urban environments is most often caused by buildings and their shadows which interfere with young street tree shapes in image scenes.

Rather than limiting tree canopy monitoring workflows to the use of one image in a classification, researchers have developed methods to merge the spectral and spatial information from multiple non-like data types into a single image classification schema through data fusion. Pixel-level data fusion is the process of compiling multiple raw data sources into single-resolution data which hosts the fused spectral and spatial data. This process is preferred when attempting to identify the relationship between variables given the incorporation of multiple input attributes into a singular final output (Zhang 2010). Alternatively, feature-level data fusion, the method this thesis employed, fuses raw input data to extract image features for combination into a final output (Zhang 2010). This approach is preferred in analyses with big data requirements, like hyperspectral imagery and LiDAR point clouds, given the user's ability to extract only the necessary pieces of information from each raw data input rather than stacking all input information into a single output (Zhang 2010). This requires an initial pixel-level classification of input data before final segmentation into image features.

Chapter 3 Methods

This thesis quantified tree canopy changes in Los Angeles using a pixel-based, object-based, deep learning, and data-fusion image classification techniques. High-resolution 60-centimeter satellite imagery, LiDAR point clouds, and building footprint polygon data were sourced from the National Agricultural Imagery Program (NAIP), LARIAC, and Los Angeles's GeoHub open data website respectively. In ArcGIS Pro, LiDAR point cloud data was then used to produce surface and terrain raster derivatives while NAIP four-band imagery was converted into an NDVI classification of vegetation. NAIP imagery was classified into seven land cover classes in ArcGIS Pro using a supervised pixel-based classification approach, a supervised object-based approach, and the ArcGIS 'Tree Segmentation' deep learning package guided by the work of O'Neil-Dunne, MacFaden, and Royar (2014) and O'Neil-Dunne et al. (2013). Additionally, LiDAR derivates were segmented into two land cover classes via OBIA, tree canopy and unclassified, and improved using contextual spectral and spatial information provided by both polygon and raster datasets in the GIS software eCognition. Each classification result was then compared via a confusion matrix using a stratified random sampling process. Information on geoprocessing time, complexity, and applicability was considered in the final determination of an ideal classification approach.

3.1 Methods Overview

The PBIA was conducted in ArcGIS Pro on 4-band NAIP imagery. First, 700 sample training data pixels were collected according to a custom 7-class land cover schema organized into tree, shrub/grass, dirt, buildings, paved ground, water, and shadow land cover classes. The image was then initially classified using the SVM classifier first into this 7-class land cover

scheme then subsequently reclassified into a two-class scheme which segmented the imagery into 'tree' and 'not tree' land cover classes.

The OBIA analysis was conducted in ArcGIS Pro on 3-band, red, green, blue (RGB) imagery derived from the previously referenced 4-band NAIP imagery as seen in Figure 6. First the image was segmented into image objects according to both the spatial and spectral similarity of pixels across the study area. Next, 700 training sample polygons were collected within the 7-class land cover schema created for the PBIA. Then, the 3-band NAIP image was classified using the SVM classifier into the 7-class scheme and finally reclassified into 'tree' and 'not tree' land cover classes.

The deep learning classification was conducted in ArcGIS Pro using the 'Tree Segmentation' deep learning package provided in the ArcGIS Pro deep learning image analyst extension. This deep learning package is served pre-trained thus eliminating the need for classifier training. Finally, the data fusion analysis is conducted in the GIS software eCognition using both NAIP 4-band imagery and sourced LiDAR point cloud data. First, the sourced LiDAR point cloud were derived into nDSM, nDTM, zDifference, and slope surface raster datasets which were then segmented into image objects according to like spectral and spatial qualities. Next, these surface rasters, as well as an NDVI raster derived from the NAIP 4-band imagery, were used to reclassify these image objects into 'tree' and 'not tree' canopy classes via a stepwise reclassification approach. Once complete, these image objects were shape refined into a final two-class land cover classification of tree cover.

Once all classification analyses were completed, all classified results raster datasets were assessed according to their classification accuracy via confusion matrix. First, stratified random sample points were created for each resultant raster. Each set of sample points were then

reclassified according to the land cover class of the image pixel that each assessment point

intersected with in both the classified image result and in the ground truth NAIP imagery. These

points were then used to compute confusion matrices for a final comparison of all classification

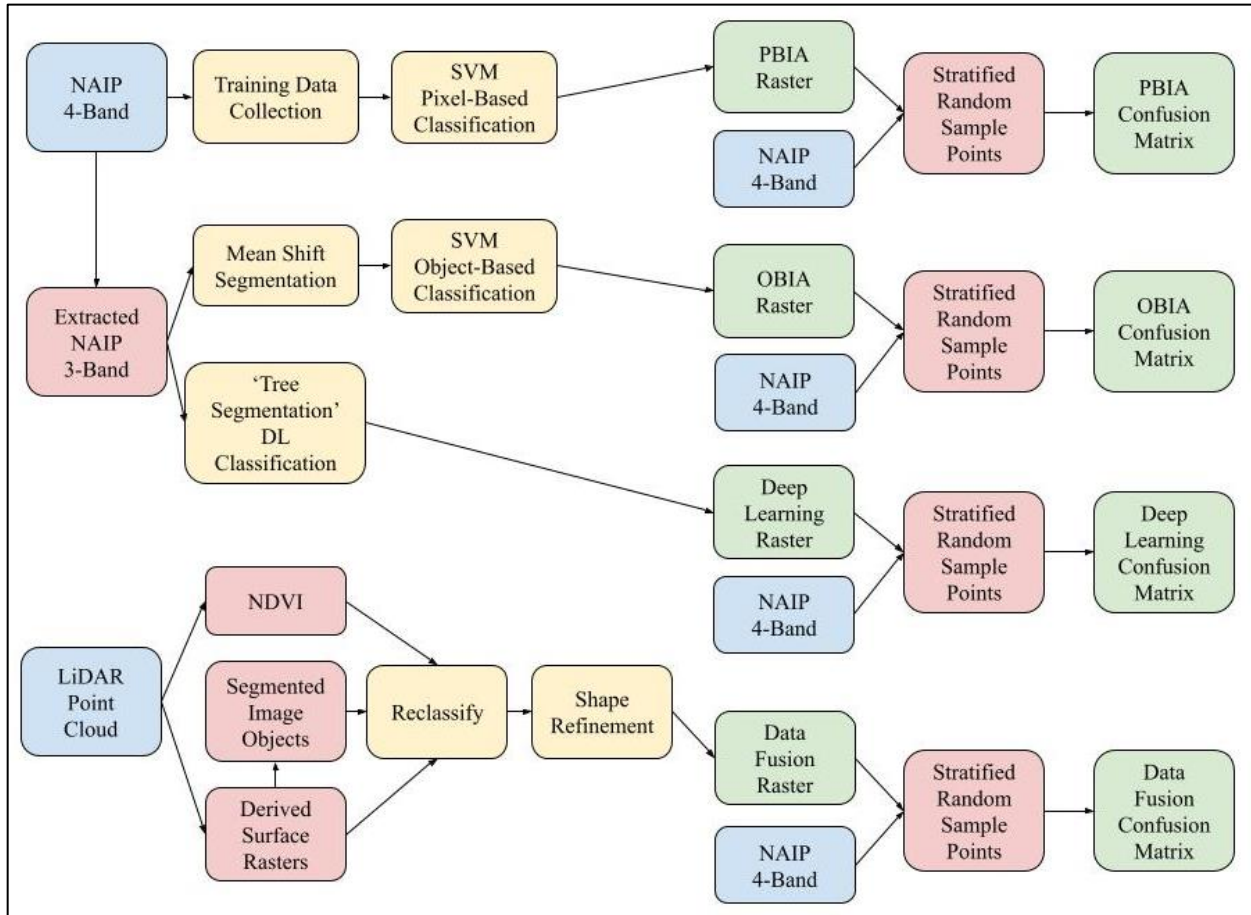types according to accuracy and agreement.

Figure 6. Thesis workflow

3.2 Software

This thesis analysis was completed using both Esri's ArcGIS Pro and Trimble's

eCognition software. ArcGIS Pro acts as the industry standard GIS program, however, requires a

purchasing license to be used. Alternative programs, like QGIS, act as suitable alternatives to ArcGIS Pro's GIS capabilities, however, ArcGIS Pro provides the benefit of its robust 3D processing capabilities which are amply suited for this analysis given its use of 3D LiDAR point cloud datasets. Additionally, ArcGIS Pro allows access to Esri's greater online GIS infrastructure making data serving far more streamlined. Thus, ArcGIS Pro's compatibility and data sharing infrastructure make it the ideal software for use in this thesis which looked to serve actionable results paired with an easily replicable workflow. Similarly, Trimble's eCognition acts as the industry standard data fusion software. Given data fusion is a relatively new advancement in GIS image classification, past analyses have developed workflows which allow for data fusion, however, must be conducted across multiple programs like ArcGIS Pro and R Studio. Thus, eCognition allows for the streamlined processing of multiple data types (vector, raster, etc.) in a singular GIS software. Additionally, eCognition workflows are saved in rule set notebooks which can be exported and shared with others. These notebooks can be immediately processed without having to manually rewrite each rule set making reiteration easier.

3.3 Data and Pre-Processing

This analysis leveraged both four-band imagery and LiDAR point data as its remotely sensed source data. Shown in Table 1, NAIP four-band imagery was collected from the California Department of Fish and Wildlife's online ArcGIS REST Services Directory which hosts all California NAIP products collected between 2005 and 2022. This 4-band imagery was used for the PBIA analysis and was extracted into a 3-band, RGB derivative which was used to complete both the OBIA and deep learning classifications. LARIAC LiDAR point clouds were collected from the NOAA: Data Access Viewer, an open data website dedicated to serving land cover, imagery, and LiDAR data. This point cloud data was derived into various 1-meter

resolution raster datasets for use in the data fusion classification of tree canopy. Both the

LARIAC and NAIP datasets were collected in 2016 according to the dataset owners, however,

visual analysis of features indicate collection likely occurred at different times of the year. All

datasets in this analysis were initially imported into an ArcGIS Pro project and reprojected into

the NAD 1983 StatePlane California V FIPS 0405 Feet projection to ensure analysis readiness.

Table 1. Data

Dataset	Description	Format	Data Type	Spatial Unit/Scale	Temporal Scale	Source
LARIAC-4 LiDAR	LiDAR point cloud	.laz	3D Point	1m	2016	LARIAC
NAIP 4-Band Imagery	60 cm resolution R, G, B, NIR band satellite imagery	.tiff	Raster	60 cm	2016	CA Department of Fish and Wildlife
LA Neighborhood Council Districts	Polygon dataset of neighborhood council district boundaries.	.shp	Vector	Feet	2015	LA GeoHub
LA Building Footprints	Polygon dataset of building footprint boundaries with attribute information on building height and elevation.	.shp	Vector	Meters	2016	LARIAC

To prepare for the data fusion the sourced LiDAR point cloud data was converted into

derivative raster datasets which described various surface feature conditions of the study area.

First the LARIAC 4 LiDAR tile grid shapefile, named 'tilegrid.shp' for analysis, was

downloaded from the LARIAC website and imported into an ArcGIS Pro project. This polygon

dataset identified thearea that each LARIAC point cloud dataset was collected. Next, the Los

Angeles neighborhood council districts dataset, named 'districts.shp,' was imported and

reprojected into the same projection. Using the select by location tool with an intersect

relationship, all LiDAR grid tiles that intersect with the study area polygon in the 'districts.shp'

layer were selected and exported into a final 'studyarea.shp' dataset. Then, each LiDAR point

cloud within this tile grid was downloaded in their served .laz file format. Each .laz file was then

converted into the compatible .lasd file format using the 'Convert LAS' tool in ArcGIS Pro.

Finally, each LiDAR .lasd file was imported into a single projected SA_LAS.las dataset for later

processing in ArcGIS Pro. This singular point cloud dataset was then derived into various raster

datasets which describe different study area surface conditions.

3.3.1 NDVI

Using the reprojected four-band NAIP imagery 'NAIP.tif' an NDVI raster was created in

ArcGIS Pro. NDVI is created by calculating the ratio of the difference between reflectance

values captured in the red (R) and near infrared (NIR) bands in four-band imagery according to

the equation below:

NDVI = (NIR reflectance – R reflectance) / (NIR reflectance + R reflectance)

This was completed in ArcGIS Pro by using the NDVI raster function on the NAIP four-

band imagery. The NDVI map in Figure 7 scores vegetative health on a numeric scale between -

1 and 1 in which positive values are considered vegetation and negative values are considered

non-natural, impervious surfaces. Based on a visual analysis of the NDVI values within the study

area, pixels with NDVI values greater than 0.2 were to be considered light vegetation or shrubs

while pixels with NDVI values greater than 0.5 were to be considered tree cover.

Figure 7. Normalized difference vegetation index

3.3.2 DEM

A digital elevation model (DEM) was created in ArcGIS Pro the LiDAR .lasd dataset

produced in pre-processing. First, a ground points LAS filter was applied to the .lasd dataset

which isolates only ground points in the LiDAR dataset. Then the final DEM was created using

the "LAS to Raster" function set with an 'AVERAGE' cell assignment type and a one-meter

pixel resolution which is equal to the sample distance of the original LiDAR point cloud thus the

finest possible output resolution. The one-meter spatial resolution output raster dataset, DEM.tif,

seen in Figure 8 captures the elevation values of the ground surface in each raster cell which was

later used to normalize other LiDAR derivative raster outputs according to the local elevations of
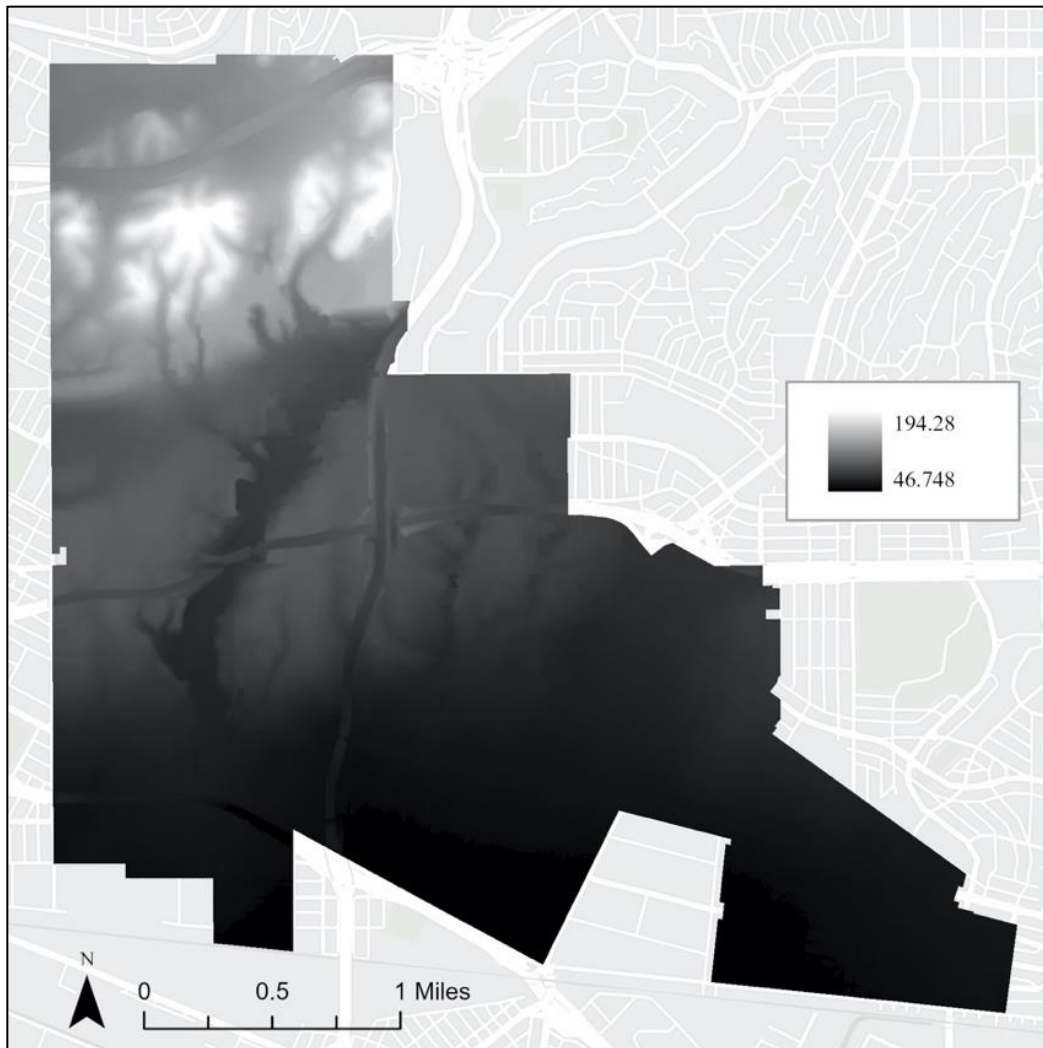
the study area.

Figure 8. Digital elevation model

3.3.3 nDSM

Next, a normalized digital surface model (nDSM), shown in Figure 9 was created in ArcGIS Pro using the LiDAR dataset produced in pre-processing and its derived DEM. First, an LAS filter was applied to SA_LAS.lasd dataset to extract first return values which fall at the top surface of the study area. The elevation values of these first return LiDAR points were then rasterized using the "LAS to Raster" tool. In the "LAS to Raster" tool settings, the cell assignment type parameter was set to 'MAXIMUM' and the output spatial resolution was set to one meter. The derived one-meter resolution raster dataset was named DSM.tif. Next, the DSM.tif dataset was normalized using the elevation values stored in the DEM.tif layer created previous. Using the raster calculator tool, the normalized DSM is derived by subtracting the DEM.tif from DSM.tif resulting in a one-meter output raster named nDSM.tif.
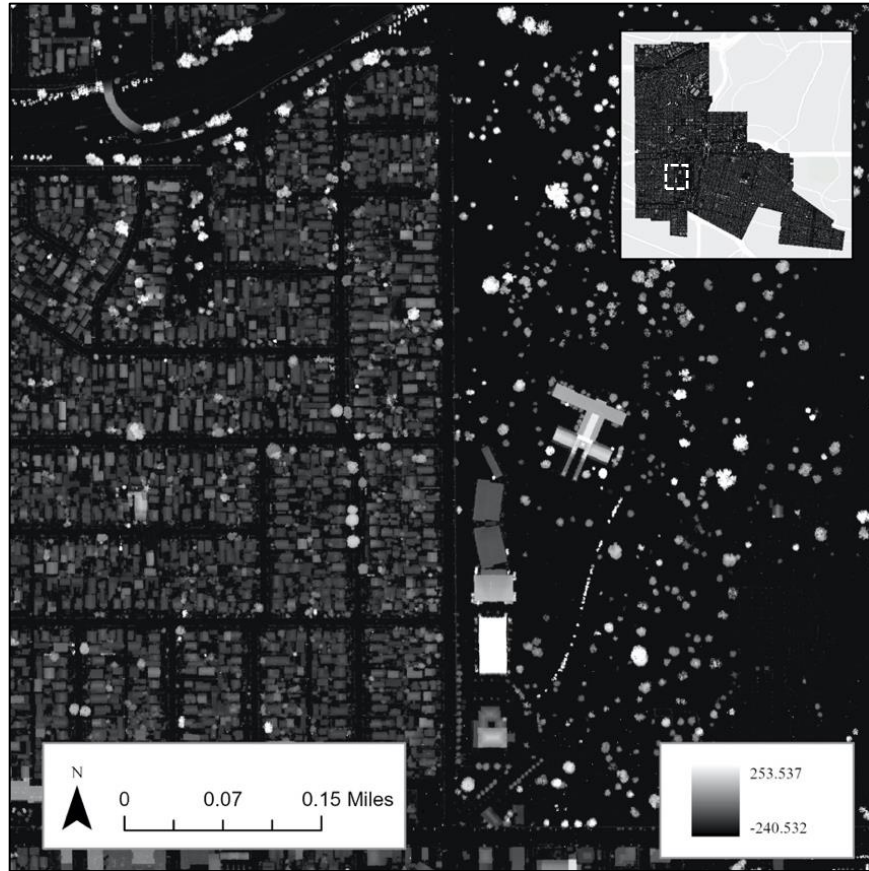
Figure 9. Normalized digital surface model

3.3.4 nDTM

A normalized digital terrain model (nDTM), shown in Figure 10 was created in ArcGIS

Pro using the SA_LAS.lasd LiDAR dataset produced in pre-processing and its derived DEM.

First, an LAS filter was applied to the .lasd dataset to extract 'last' return values which fall at the

bottom of the LiDAR point cloud. Then the "LAS to Raster" function was used to rasterize these

'last' return values into a DTM. In the tool settings the cell type assignment parameter was set to

'MAXIMUM' and the output spatial resolution is set to one meter. This creates a one-meter

raster output DTM labeled DTM.tif. Finally, this output DTM was normalized using the raster

calculator tool to divide the DTM.tif raster by the DEM.tif to produce an output nDTM named
nDTM.tif.
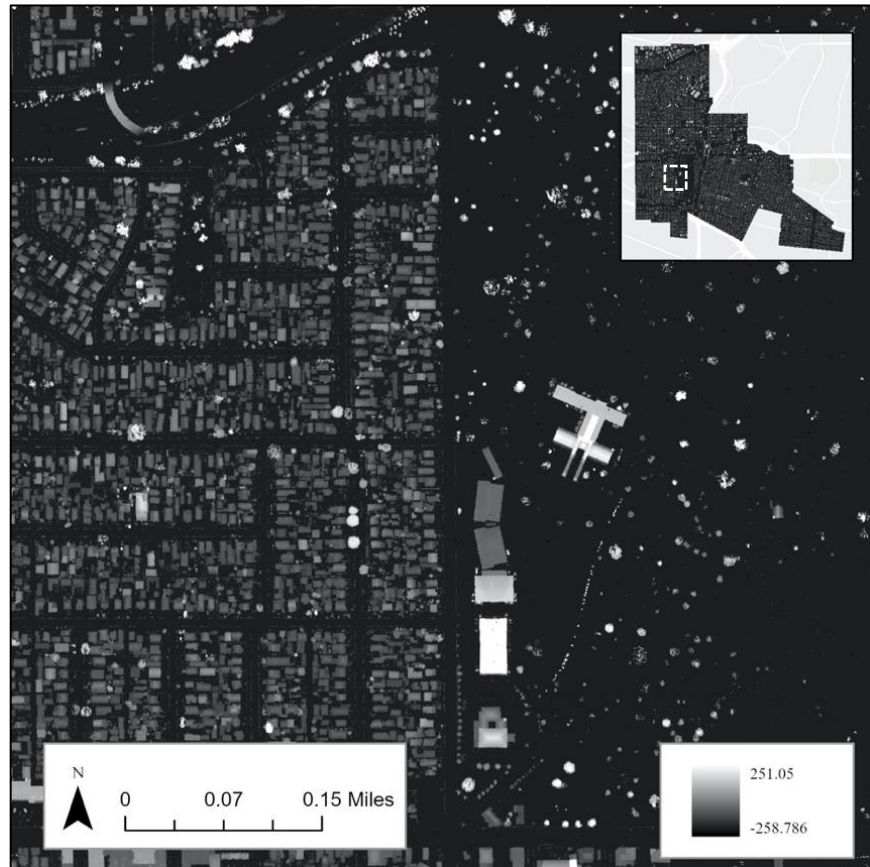
Figure 10. Normalized digital terrain model

3.3.5 *zDifference*

A zDifference dataset was created in ArcGIS Pro using the nDSM.tif and nDTM.tif raster
datasets derived from LiDAR imagery previous. Using the "Raster Calculator" function, the
nDTM.tif was subtracted from the nDSM.tif which produced a one-meter raster output titled
zDifference.tif. The values stored in the raster output indicate the difference in the elevation
between first and last return LiDAR points. Clusters of pixels with large zDifference values are

to be considered canopy given their loose canopy foliage allows for LiDAR sensors to penetrate to the ground surface whilst clusters of pixels with small zDifference are likely buildings given that the LiDAR cannot penetrate their impervious roof structure (O'Neil-Dunne et al. 2013). This is confirmed in a visual analysis of the raster output seen in Figure 11.
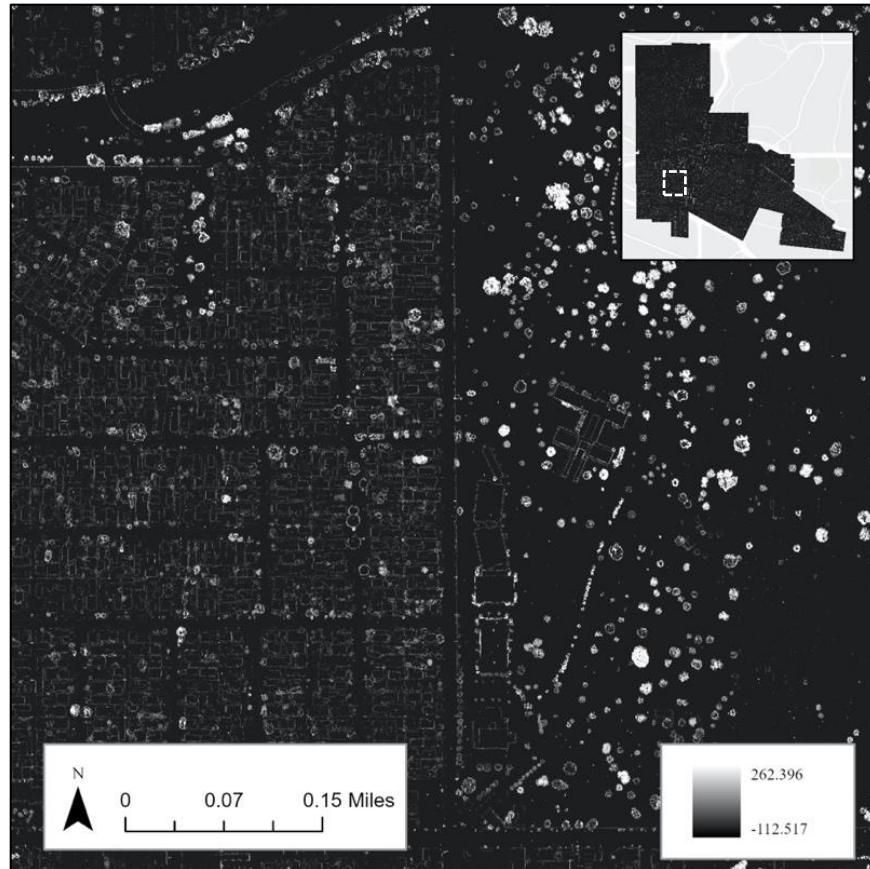
Figure 11. zDifference

3.3.6 Slope

A slope dataset, titled slope.tif, was created using the nDSM.tif raster created in section 3.1.3 and the 'Slope' tool found in the ArcGIS Pro Spatial Analyst toolkit. The output measurement parameter was set to 'degree' whilst all other tool parameters remain default. The

result was a one-meter resolution raster dataset which captures degrees slope in each raster pixel.

As seen in Figure 12, trees are identified as round batches of white pixels given their variable

canopy structure returns high slope values whilst buildings are identified as black rectangular

polygons outlined with white, high slope pixels given their flat roof structure constitutes low

slope returns.
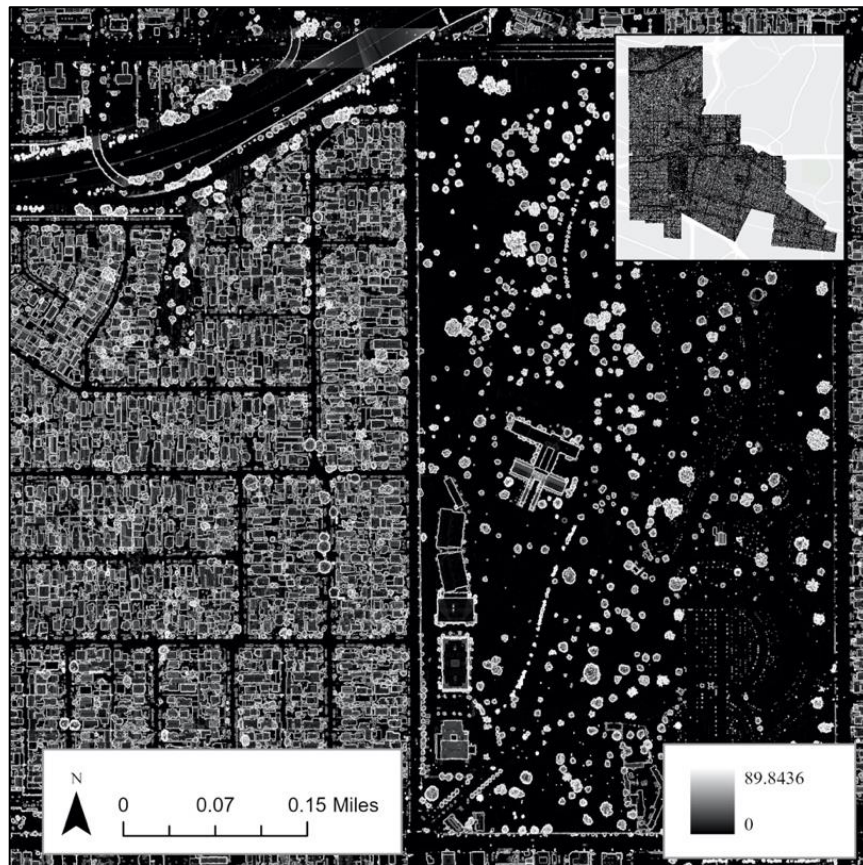
Figure 12. Slope

3.4 Supervised Pixel-Based Classification

Supervised pixel-based classification was conducted in the ArcGIS Pro Imagery Wizard

on the 60-centimeter four-band NAIP imagery sourced for this analysis. First, a seven-class land

cover schema was created to describe all desired land cover domains in the study area upon which 100 training sample pixels were collected per land cover class. The Support Vector Machine (SVM) classifier was then applied to produce a one-meter resolution raster image product. Finally, this raster product was reclassified into two land cover classes classes, 'tree' and 'not tree', for a later assessment of accuracy.

3.4.1 Training Data Collection

First, the Training Sample Manager in the ArcGIS Pro classification tools was opened whilst the 2016 NAIP imagery was selected in the contents pane of the map project. This ensured that the NAIP imagery was used as the input for training sample collection. Next, as seen in Figure 13 a new land cover schema in the training samples manager was created. This schema captured seven land cover classes: tree, shrub/bush, dirt, building, paved ground, shadow, and water. This schema is then exported into an Esri Classification Schema (.ecs) file entitled schema.ecs for use in the final classification.
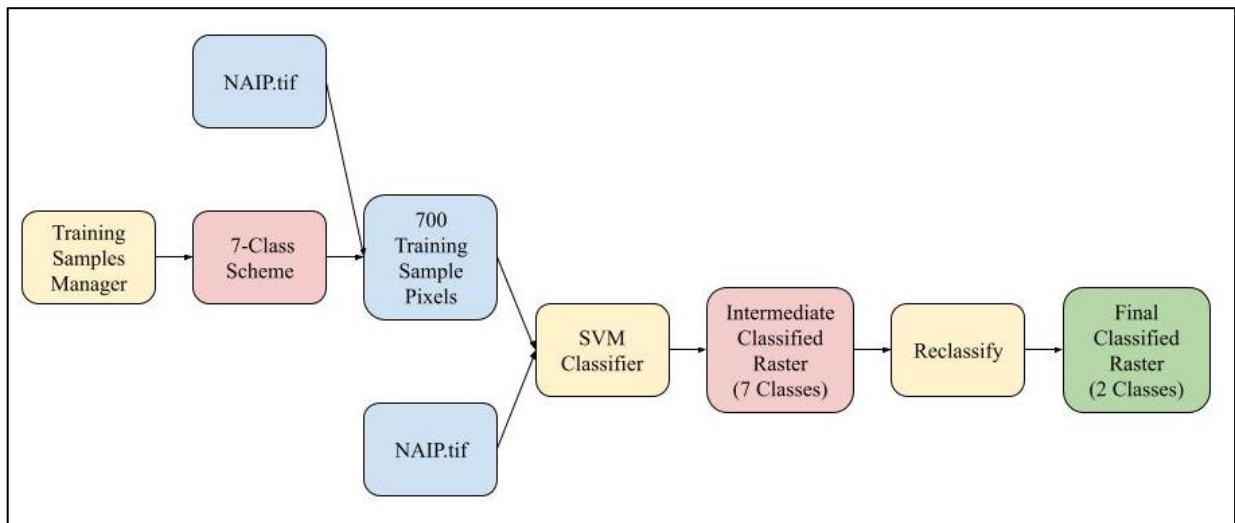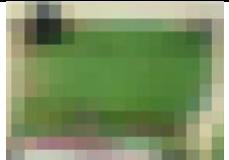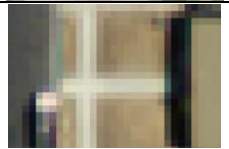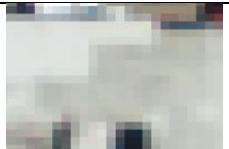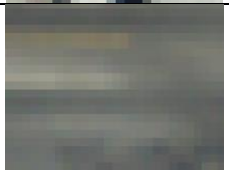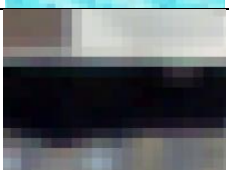
Figure 13. PBIA workflow

Next, using the pixel selection tool in the training samples manager, 100 training sample pixels per land cover class were identified in the image scene. Table 2 describes the characteristics of each land cover class within the image scene and provides figures of sample training pixels identified for each class. Given a PBIA leverages the reflectance values and RGB intensity of training data sample pixels in the final classification, capturing a large range of pixel colors and types was prioritized. For example, in the tree canopy class, training sample pixels included both dark green tree canopies that which belonged to healthy trees with a denser canopy as well as lighter yellow and brown pixels which belonged to trees with less dense and 'non-traditional' canopy structure. Additionally, pixels in the most exposed part of the trees and pixels in the dark, shaded portions of the tree canopy were selected to ensure shaded holes in the canopy were not ignored in the classification result. Once training sample collection was complete, all training samples were exported into an independent vector point dataset (.shp) entitled PBIA_samples.shp.

Table 2. PBIA land cover class pixel characteristics

Land Cover Class	Image Characteristics	Sample Data
Tree Canopy	Circular groupings of pixelated green pixels	
Grass/Shrub	Angular groupings of contiguous green pixels, often found in yards or sidewalks	
Dirt	Angular groupings of contiguous brown pixels, often found in yards or sidewalks	
Buildings	Rectangular groupings of white and gray pixels which define rooftops	
Paved Ground	Contiguous linear groupings of dark gray, light, gray, and white pixels in the road and sidewalk network	
Water	Contiguous angular groupings of blue and light blue pixels	
Shadow	Circular and angular groupings of dark black pixels found adjacent to trees and building footprints	

3.4.2 Classification Parameters

Finally, the PBIA classification was completed using the 'Classify' tool in the ArcGIS

Pro classification toolkit. Before the 'Classify' tool was opened, the NAIP four-band imagery

was selected in the project contents to ensure its use as the input for classification. First in the

classify tool, the classification method parameter was set to supervised, which mandates the use

of training samples, and the classification type parameter is set to pixel based. Next, the seven-class land cover schema described previously was assigned to the classification which ensures that the result image is separated into these seven classes. Then the training samples data created for this classification previous, PBIA_samples.shp, were assigned to the training samples parameter in the classify tool. Finally, the SVM with a constraint maximum number of 500 samples per class was assigned as the final parameters of the 'classify' tool at which point the tool was prompted to classify and export the resultant raster image: PBIA.tif.

3.5 Supervised Object-Based Classification

Supervised object-based classification was conducted in the ArcGIS Pro Imagery Wizard on the four-band NAIP imagery sourced for analysis. First, the MeanSegmentShift tool was applied on the imagery to derive image objects for classification. Using the same seven-class land cover scheme created for the PBIA, 100 training sample objects per image class were chosen using polygon object selector within the ArcGIS Pro training samples manager. Next, the NAIP imagery was classified using the SVM classifier trained on the sample objects collected. Last, the output was reclassified into a two-class land cover classification. The final product is a one-meter resolution raster classified into 'tree' and 'not tree' classes.

3.5.1 Segmentation

First the 2016 four-band NAIP imagery used for this analysis was extracted into a derivative 3-band image using the 'Extract Bands' raster function to ensure data compatibility with the classifier. The input raster parameter was set to the 2016 NAIP imagery, the method parameter was set to 'Band IDs' and the band combination is set to '1 2 3' which selects the 1, 2, and 3 (red, green, and blue) for extraction. The output of this tool was a three-band raster image

entitled NAIP_3band.tif with the same spatial extent, resolution, and projection of the original four-band imagery but limited to only the red, green, and blue bands.

Before training data collection, the input three-band NAIP imagery was segmented into image objects using the 'Segment Mean Shift' tool which segments input raster imagery into groups according to similarities in their spectral and spatial characteristics. The spectral detail parameter of the tool defines the level of importance that spectral features, like color and reflectance, have on the final segmentation in a value range between 1 and 20. Higher spectral detail parameter values are chosen to produce more a more contrasted segmented output when multiple, separate object features share spectral characteristics while lower parameter values are chosen to create smoother outputs and perform better when object features have less like spectral characteristics. A spectral detail value of 16.7 was chosen given the spectral diversity of the image to ensure separation between natural objects, like trees and lawns, and nonnatural objects, like buildings and road surfaces.

The spatial detail parameter defines the level of importance that feature proximity has on segmentation. Higher spatial detail values are ideal for image scenes with small, clustered object features while lower detail values result in smoother output segmentation. Given the small size and near proximity of tree, building, and built environment features being segmented in the NAIP imagery, a spatial detail value of 16 was chosen to create a more detailed output. The result is a segmented raster dataset, entitled SegmentedNAIP.tif,

3.5.2 Training Data Collection

As seen in Figure 14, the training samples manager tool in the ArcGIS Pro classification tools was opened whilst the NAIP_3band.tif imagery was selected in the contents pane of the map project. This ensured that the three-band NAIP imagery derived previous was used as the

input for training sample collection. Next, the seven-class land cover schema created for the

previous PBIA, schema.ecs, is opened in the training samples manager. This ensures the land

cover classes used for the OBIA mimics that of the PBIA for the sake of later comparison.
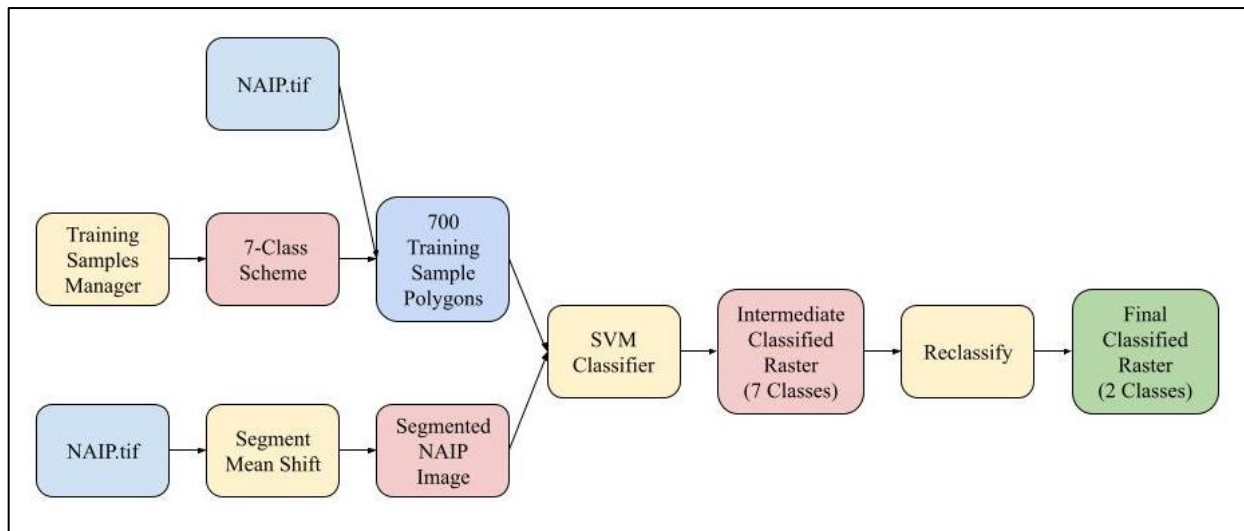
Figure 14. OBIA workflow

Next, using the linear, circle, and freehand polygon selection tools in the training samples

manager, 100 training sample polygons per land cover class were identified in the image scene.

Table 3 describes the characteristics of each land cover class within the image scene and

provides figures of sample polygons identified for each class. Once training sample collection

was complete, all training samples were exported into an independent vector point dataset (.shp)

entitled OBIA_samples.shp.

Table 3. OBIA land cover class pixel characteristics

Land Cover Class	Image Characteristics	Sample Data
Tree Canopy	Circular groupings of pixelated green pixels	
Grass/Shrub	Angular groupings of contiguous green pixels, often found in yards or sidewalks	
Dirt	Angular groupings of contiguous brown pixels, often found in yards or sidewalks	
Buildings	Rectangular groupings of white and gray pixels which define rooftops	
Paved Ground	Contiguous linear groupings of dark gray, light, gray, and white pixels in the road and sidewalk network	
Water	Contiguous angular groupings of blue and light blue pixels	
Shadow	Circular and angular groupings of dark black pixels found adjacent to trees and building footprints	

3.5.3 Classification Parameters

Finally, the OBIA classification was completed using the 'classify' tool in the ArcGIS

Pro classification toolkit. Before the 'classify' tool was opened, the NAIP three-band imagery,

NAIP_3band.tif, was selected in the project contents to ensure its use as the input for

classification. First in the classify tool, the classification method parameter was set to supervised,

which mandates the use of training samples, and the classification type parameter was set to

object based. Next, the seven-class land cover schema, schema.ecs, was assigned to the

classification which ensures that the result image is separated into these seven classes. Then, the

training samples data created for this classification previously, OBIA_samples.shp, were

assigned to the training samples parameter in the classify tool. Finally, the SVM with a

constraint maximum number of 500 samples per class was assigned as the final parameters of the

'classify' tool at which point the tool was prompted to classify and export the resultant raster

image: OBIA.tif.

3.6 Deep Learning Classification

The deep learning classifier used to accomplish this analysis was the 'Tree Classification'

deep learning classifier developed by the Esri analytics team and was applied in ArcGIS Pro to

identify tree canopy polygons in 2016 NAIP imagery. This polygon output was then rasterized

and derived into a raster dataset which classified tree canopy into the same 'tree' and 'not tree'

land cover classes used in the PBIA and OBIA classifications for the sake of later comparison.

3.6.1 Classification

First, the deep learning classifier .dpk file was downloaded out of the ArcGIS Living

Atlas catalog and stored to a location on the local drive of the computer used for this thesis.

Next, given the required input data of the model is three-band imagery, the four-band NAIP

imagery sourced for this analysis was converted into an appropriate three-band alternative. Using the 'extract bands' tool found in the ArcGIS Pro raster functions toolkit, bands 1, 2, and 3 of the NAIP imagery (the red, green, and blue bands) were extracted and merged into a new composite three-band image for deep learning classification. Once the input was properly prepared, the tree segmentation model was run using the 'Detect Objects Using Deep Learning' tool in the ArcGIS Pro Image Analyst toolkit. The input raster was set to the newly created three-band NAIP imagery and the model definition is set to the pathway which leads to the location of the tree classification deep learning .dpk file on the local computer with all other settings remaining default. This created a vector layer which identified tree canopy through polygons.

3.6.2 Rasterization

To prepare this output for a pixel-based accuracy assessment, rasterization into the 'tree' and 'not tree' land cover classes was required. To create the 'not tree' region to contrast the tree canopy polygons, the erase tool, with the input being the studyarea.shp study area polygon and the erase features being the deeplearningtree.shp polygons, was used to erase the tree canopy areas from the study area polygon resulting in a 'not tree' polygon. Next, in the fields view of both the 'tree' and 'not tree' polygon layers a like 'CLASS' text field was created to store the assigned layer classification. In the deeplearningtree.shp layer the 'calculate field' function was used to assign the text 'tree' in the CLASS field. Then in the studyarea.shp layer the 'calculate field' function was used to assign the text 'not tree' in the CLASS field. This ensured that each datasets classification is hosted in the attribute information of each layer. Next, the 'merge' tool was used to join the deeplearningtree.shp and studyarea.shp layer inputs into a single polygon dataset deeplearningpolygons.shp. The result was a spatially contiguous polygon dataset which classified 'tree' and 'not tree' area in the previously added and now merged 'CLASS' field. To

complete rasterization, the 'polygon to raster' tool was used to convert the deeplearningpolygons.shp layer into a raster classification for later accuracy assessment. In the tool parameters, the original NAIP.tif imagery was assigned as the snap raster which ensured that the rasterized output of the deeplearningpolygons.shp layer mimics the spatial resolution, extent, and projection of all other data in this analysis.

3.7 Data Fusion Classification

The data fusion OBIA in this thesis was conducted in the Trimble GIS software eCognition. The stepwise approach applied in the segmentation and reclassification process was adopted from methods developed in O'Neil-Dunne, MacFaden, and Royar (2014) and O'Neill-Dunne et al. (2013) which call for a data fusion OBIA built on initial classifications of high-resolution LiDAR imagery. An initial object-based classification was followed by the incorporation of raster then vector data in a data fusion process which reclassified initially misclassified pixels according to spectral and spatial properties of supplementary data. Initial fusion steps incorporated high-resolution raster data due to their minimal parallax effects which minimize classification speckling and pixel mixing whilst still initially 'over classifying' tree canopy. Next, higher-resolution raster data, like NDVI, is introduced into the data fusion which is followed by a final vector data incorporation to fix the initial misclassification of built environment pixels as vegetation.

3.7.1 Segmentation

Initial segmentation began with the multiresolution segmentation of imagery into object shapes. First a rule set with the multiresolution segmentation algorithm was created which considered slope, zDifference, nDTM, and nDSM values in its determination of image objects. Each image layer was assigned the default layer weight value of one aside from the nDSM layer

which was assigned a layer weight of three which increases the influence of values in the deciding of image objects. The nDSM was weighted the heaviest as its high image and pixel value contrast best differentiate object features. The scale factor parameter, which defines the size of objects identified in the image scene between one and infinity with larger values correlating with larger objects, was assigned a value of five, rather than the default 10, to both ensure that smaller object features in the image are captured and that larger obect features are segmented into smaller objects which can be accurately reclassified into tree objects. The compactness factor, which defines object compactness on a scale from 0 – 1.0 with higher values resulting in more compact segmented features, was assigned a value of 0.9, greater than the default of 0.1, to ensure compact and editable image objects. Finally, the shape parameter was assigned a value of 0.9 which is greater than the default value of 0.5. This parameter defines the influence object shape has on final segmentation with higher values within the range from 0 – 1.0 indicating a higher shape influence than color influence in the final object segmentation.

3.7.2 Refinement

Once object segmentation was complete, the newly created image objects were classified into 'tree' and 'other' object classes using the 'assign class' ruleset. First, all image objects with a mean nDSM value greater than or equal to two meters, according to the nDSM.tif layer, were assigned to the tree class. As seen in Figure 15, this assigned all object features that are taller than two meters to the tree class creating a base 'over' classification which can be edited using values in other .tif imagery layers.
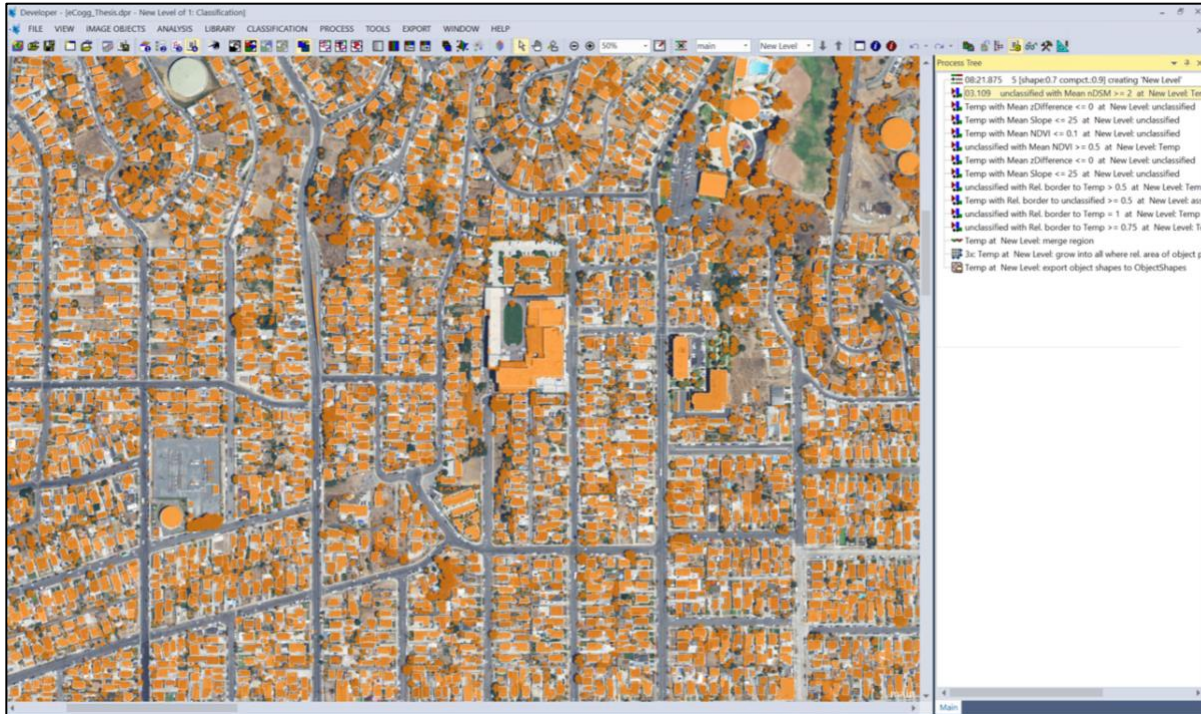
Figure 15. Intermediate nDSM classification

Next, all image objects newly assigned to the 'tree' class with a mean zDifference value less than or equal to 0 according to the zDifference.tif image layer were reassigned to the 'not tree' class. This is due to the assumption that any pixels with no difference in first and last return height values are likely flat, impervious surfaces, like buildings, and should be classified as 'other.' Next, all 'tree' image objects with a mean slope less than 25 degrees, according to the values stored in the Slope.tif image layer, were assigned back to the 'not tree' class. This was done under the assumption that any features with flat slope can be assumed to be a manmade object and is confirmed through an inspection object slope values in the image scene. Finally, 'tree' objects with a mean NDVI value less than or equal to 0.1 are assigned to the 'other class.' This is according to an inspection of the NDVI values of objects in the image scene and the assumption that image pixels with NDVI values less than 0.2 are non-vegetative. Once this initial

47

set of object classification rules was complete, further classification was repeated to refine the accuracy of the image classification.

First, all 'other' object with a mean NDVI value greater than or equal to 0.5 were assigned to the 'tree' class. Next all 'tree' objects with a mean zDifference greater than or equal to 0 were reassigned to the 'not tree' class. Next, all 'tree' objects with a mean slope less than or equal to 25 degrees were assigned to the 'not tree' class. Next, any 'other' objects comprised of less than 35 pixels and that shared more than 50% of their boundary with 'tree' objects were reclassified to the 'tree' class. As seen in Figure 16, this was meant to fill any holes in tree canopy objects which had been misclassified as 'not tree.'
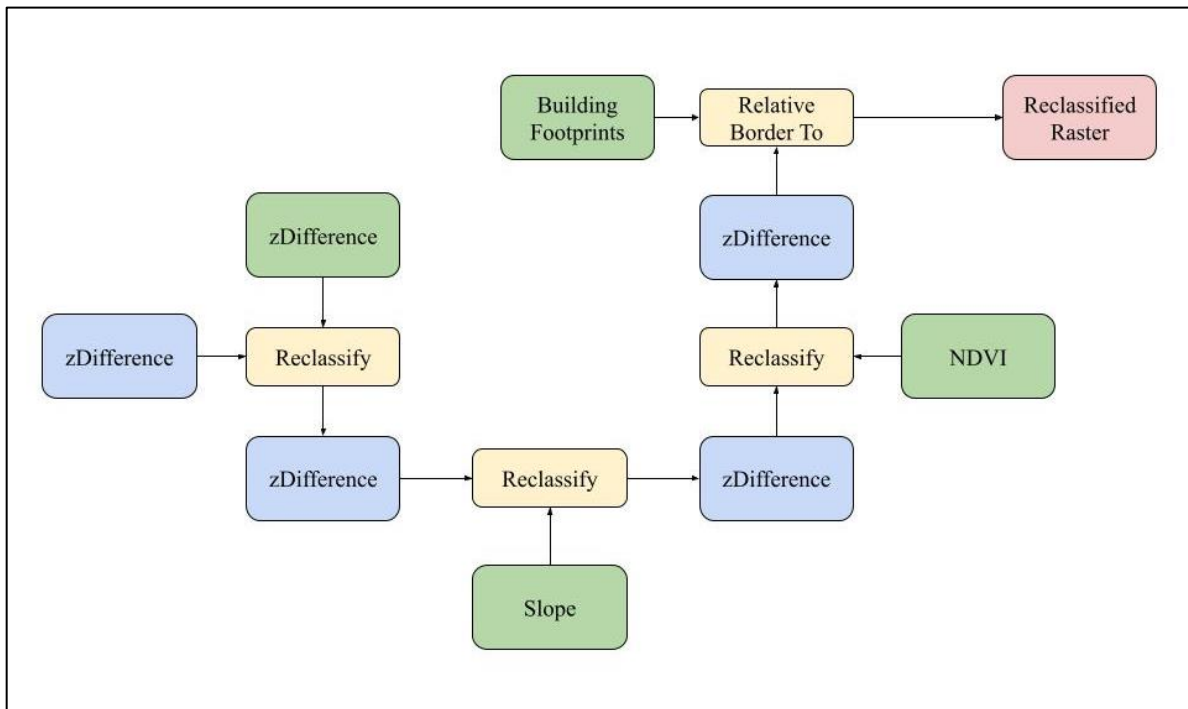
Figure 16. Stepwise data fusion workflow

3.7.3 Vector Incorporation and Object Resizing

Once raster reclassification was complete, building footprint vector data was imported into the eCognition for further reclassification. Using the 'assign class by thematic layer' tool with the building footprint vector layer, all 'tree' objects that shared more than 50% of their border with 'other' objects within the polygon boundary of the building footprints vector layer were reclassified to 'not tree.' This was done to fix any tree objects that have been misidentified within known building footprint boundaries. Next, all 'other' objects that shared 100% of their border with 'tree' objects were assigned to the tree class to further fill holes in the classification. This was repeated twice more with all 'not tree' objects which share over 75% of their boundary with 'tree' objects. At this point, all 'tree' object features were joined together using the 'merge region' tool resulting in whole tree canopy object features. Finally, the pixel-based object resizing tool was used on the newly joined 'tree' class to round out tree shapes and smooth object boundaries. After the reference was set to object, all candidate surface tension settings were left at their default values except for the 'Value' parameter which was increased from 0.2 to 0.5. The result was exported into a raster dataset 'eCognition.tif' which was stored locally for a later accuracy assessment in ArcGIS Pro.

3.8 Accuracy Assessment

To compare each classification approach, this thesis conducted a per-pixel based accuracy assessment for each classification output via a stratified random point sampling method. These classifications were then compared against a ground truth image using a confusion matrix which assesses classification accuracy according to Type I error (false positives), Type II error (false negatives), and a kappa statistic which quantifies the agreement of each classification with the ground truth imagery. Additionally, this thesis considered

geoprocessing times, methodological complexity, and data suitability in its decision of an ideal classification method.

First, the supervised pixel-based classification output was accuracy assessed in ArcGIS Pro using the 'Create Accuracy Assessment Points' tool. The tool input was set to the final pixel-based classification image layer PBIA.tif with the sampling method parameter set to stratified random and the number of output points set to 1,250. The result of this was a set of stratified random sampling points for the PBIA.tif image with hosted value fields, 'CLASSIFIED' and 'GROUNDTRUTH'. The ground truth field comes unpopulated while the 'classified' field hosts the classification of the sample point according to the land cover class of the image pixel with which it intersects. Thus, if a given sampling point overlaps with a 'tree' pixel in the classified PBIA.tif image, its 'CLASSIFIED' field value will be 'tree' whereas if it overlaps with a 'not tree' pixel it will be assigned the value 'not tree.' Given that the sampling method was stratified random, the number of sampling points which were pre-classified to the 'tree' and 'not tree' class in the CLASSIFIED field were proportional to the percent area of each land cover class in the classified image. This resulted in 100 sample points with a 'tree' classification and 1,150 'not tree' sample points in the CLASSIFIED field. Next, to populate the GROUNDTRUTH field, each accuracy assessment point was manually classified through visual assessment into a 'tree' or 'not tree' delineation according to the stock NAIP imagery used for this analysis. Once both the CLASSIFIED and GROUNDTRUTH fields are populated the 'Compute Confusion Matrix' tool was used to create an output confusion matrix for assessment.

This process of creating, classifying, and assessing accuracy assessment points for the PBIA classification result was replicated for the output of each classification approach to ensure a means of comparison. Given the stratified random sampling method used determined the

number of pre-classified accuracy assessment points proportional to the area of each land cover

class in the classified image, each classification's accuracy assessment required a different

number of total accuracy assessment points to ensure enough assessment points. The intent was

to have 100 'tree' class assessment points per set. Thus, each accuracy assessment was

completed with the number of points seen in Table 4.

Table 4. Accuracy assessment sample point count

Classification	Number of Assessment Pixels
PBIA	1250
OBIA	1250
Deep Learning	1500
Data Fusion	1250

Finally, the 'Compute Confusion Matrix' tool was used with the fully classified accuracy

assessment points as inputs to create final confusion matrix with which the accuracy of the pixel-

based classification of tree canopy can be assessed. This tool returned a standalone table in

ArcGIS Pro which described the user and producer accuracy of the classification of each land

cover class as well as a kappa statistic on the agreement between the classified image and ground

truth imagery. User accuracy describes type one error which shows false positives in which

pixels which do not belong to the desired land cover class are misclassified as another class. In

this instance, this would be non-tree canopy pixels in the NAIP imagery which have been

misclassified as tree canopy or tree canopy pixels in the NAIP imagery which have been

misclassified as non-tree canopy. User accuracy is calculated by dividing the number of pixels in

the classified image belonging to a land cover class by the number of pixels belonging to the

same class in the ground truth imagery. Producer accuracy describes type two error, or false

negatives, in which pixels belonging to the desired land cover class in the ground truth imagery are misclassified. Producer accuracy is calculated by dividing the number of misclassified pixels in the confusion matrix by the total number of classified pixels in this class. The Cohen's kappa statistic scores the agreement between both classified images on a numeric scale from 0 to 1 with larger values indicating higher agreement (McHugh 2012).

This accuracy assessment process was repeated three more times using the results raster produced from the supervised OBIA in ArcGIS Pro, the deep learning classification, and the OBIA fusion in eCognition. This resulted in the creation of four confusion matrices which describe the accuracy of each classification for comparison.

Chapter 4 Results

Each image classification methodology produced a 60-centimeter resolution raster dataset classified into 'tree' and 'not tree' land cover classes. By dividing the area of tree pixels by the total area of the study area, tree canopy cover was estimated to be approximately 8.7% of the study area. Based on a per-pixel stratified random sample-based accuracy assessment of each result, each classifier was judged according to the user and producer accuracy of the classification of both the 'tree' and 'not tree' land cover class.

4.1 Supervised Pixel-Based Classification

The result of the supervised pixel-based classification was a 60-centimeter spatial resolution raster image of the study area which is classified into 'tree' and 'not tree' land cover classes. As seen in Figure 17, the 'tree' land cover class was colored in green (HEX#38A800) whilst the 'not tree' areas are left transparent. Using the 'Extract by Attribute' tool, the number of raster pixels in the 'tree' land cover class was identified and divided by the total number of pixels in the study area to determine percent area of tree canopy. Then, by dividing the count of tree canopy pixels by the total number of pixels in the study area it was determined that the pixel-based classification of tree canopy identified 8.5% of the image scene as tree canopy, or 0.63 square miles.

Figure 17. Supervised pixel-based tree canopy classification

The result of the 'create confusion matrix' accuracy assessment tool was a standalone

table in ArcGIS Pro which described the user and producer accuracy each land cover

classification as well as a kappa statistic on the agreement between the classified PBIA.tif image

and the ground truth NAIP.tif image. User accuracy describes type one error which shows false

positives in which pixels which do not belong to the desired land cover class in the ground truth

image are misclassified in the classified imagery. In this instance, this described non-tree canopy

pixels in the NAIP imagery which have been misclassified as tree canopy. This could also

describe tree canopy pixels in the NAIP imagery which have been misclassified as non-tree canopy. User accuracy is calculated by dividing the number of pixels in the classified image belonging to a land cover class by the number of pixels belonging to the same class in the ground truth imagery. Producer accuracy describes type two error, or false negatives, in which pixels belonging to the desired land cover class in the ground truth imagery are misclassified. Producer accuracy is calculated by dividing the number of misclassified pixels in the confusion matrix by the total number of classified pixels in this class. The Cohen's kappa statistic scores the agreement between both classified images on a numeric scale from 0 to 1 with larger values indicating higher agreement (McHugh 2012). Table 5 describes agreement depending on the value range of the returned kappa statistic.

Table 5. Kappa statistic agreement interpretation. From McHugh (2012)

Kappa Statistic	Level of Agreement
0.01 – 0.2	No/Slight Agreement
0.21 – 0.4	Fair Agreement
0.41 – 0.6	Moderate Agreement
0.61 – 0.8	Substantial Agreement
0.81 – 1.0	Perfect Agreement

According to the accuracy assessment of the supervised PBIA classification, total classification accuracy is 95.5%. Although this points to a marginally successful classification result, an inspection of the disparity of classification accuracies between 'tree' and 'not tree' classes reveal complications. Given that overall accuracy is expressed as the dividend of correctly classified accuracy assessment and total assessment points used, any bias in classification accuracy per land cover class is hidden. Inspection of the type one and type two

errors in this classification reveal that the PBIA more accurately classified the 'not tree' land cover class.

According to Table 6, he user accuracy of the classification of the 'tree' land cover class was 73.6%. This is given the moderate rate of false positive classifications as 28 of the 106 accuracy assessment points which were misidentified as 'tree' in the classified PBIA image instead belonged to the 'not tree' class according to the ground truth NAIP imagery. In contrast, the 'not tree' land cover class returned a user accuracy of 97.8%. This is given that only 41 of the 1400 accuracy assessment points classified as 'not tree' according to the PBIA image instead belonged to the 'tree' class according to NAIP ground truth imagery. This disparity in the percent producer accuracy of classification between 'tree' and 'not tree' classes was mimicked in the PBIA producer accuracy results. The producer accuracy of the 'tree' land cover class was 75.7% due to the high rate of false negative classifications. Of the 103 accuracy assessment points which belong to the 'tree' class according to the ground truth NAIP imagery, 25 were misclassified as 'not tree' in the PBIA imagery. This is contrasted by a 97.6% producer accuracy of the 'not tree' class given only 28 false 'tree' classifications in the OBIA result relative to the ground truth imagery.

The kappa statistic value of 0.72 returned by the accuracy assessment of the PBIA describes the classified image as having substantial agreement with the ground truth imagery, however, the disparity between the kappa statistic and overall accuracy values suggests inconsistent classification performance which undermines the quality of the resultant classification (McHugh 2012).

Table 6. PBIA accuracy assessment confusion matrix

	Tree	Not Tree	Total	User Accuracy
Tree	78	28	106	73.6%
Not Tree	25	1119	1144	97.8%
Total	103	1147	1250	N/A
Producer Accuracy	75.7%	97.6%	N/A	Overall Accuracy: 72.3%

4.2 Supervised Object-Based Classification

The result of the supervised object-based classification was a 60-centimeter spatial resolution raster image of the study area which is classified into 'tree' and 'not tree' land cover classes. As seen in Figure 18, the 'tree' land cover class was colored in green (HEX#38A800) whilst the 'not tree' areas are left transparent. Using the 'Extract by Attribute' tool, the number of raster pixels in the 'tree' land cover class was identified and divided by the total number of pixels in the study area to determine percent area of tree canopy. It was determined that the object-based classification of tree canopy identified 6.7% of the image scene as tree canopy, or 0.50 square miles.
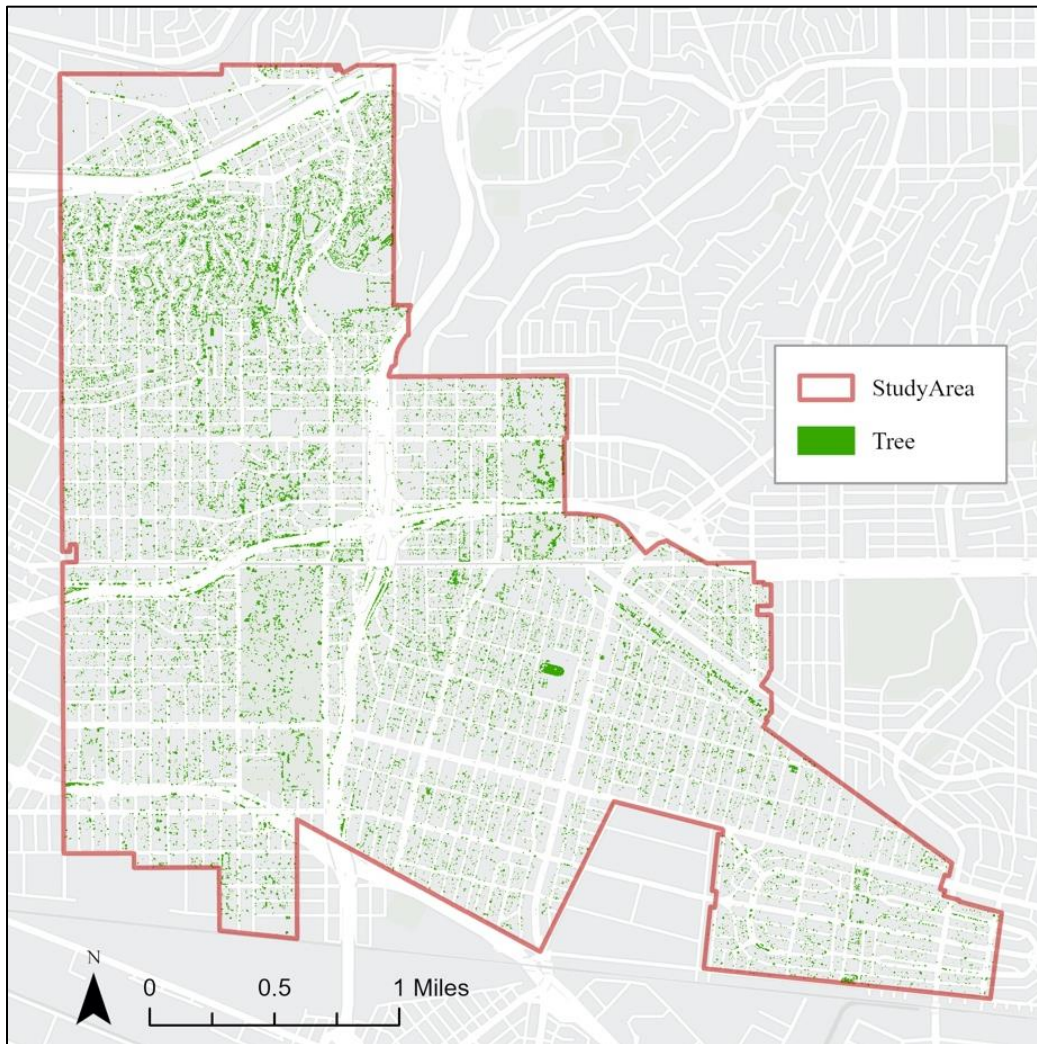
Figure 18. Supervised object-based tree canopy classification

According to the accuracy assessment of the OBIA classification of tree canopy, overall classification accuracy was 96.5%. This suggests a successful classification given a classification accuracy result greater than 90%. However, a significant disparity in the producer accuracy between the 'tree' and 'not tree' land cover classes suggest a less consistent result.

According to Table 7, the user accuracy of the classification of the 'tree' land cover class is 88.0%. This is given the moderately low rate of false positive classifications as 12 of the 100 accuracy assessment points which were misidentified as 'tree' in the classified OBIA image and

instead belonged to the 'not tree' class according to the ground truth NAIP imagery. In contrast, the user accuracy of the 'not tree' land cover class is 97.1%. This is given that only 41 of the 1400 accuracy assessment points classified as 'not tree' according to the OBIA image are false negative classifications and instead belong to the 'tree' class according to ground truth imagery. However, the disparity in the percent producer accuracy of classification between 'tree' and 'not tree' classes is greater than the disparity in user accuracies. The producer accuracy of the 'tree' land cover class is 68.6% due to the high rate of false negative classifications. Of the 129 accuracy assessment points which belong to the 'tree' class according to the ground truth NAIP imagery, 41 of which were misclassified as 'not tree' in the OBIA imagery. This is contrasted by a 99.1% producer accuracy of the 'not tree' class given only 12 false 'tree' classifications in the OBIA result relative to the ground truth imagery.

Given the disparity in classification accuracies per land cover class, the kappa statistic of this classification assessment can be used to provide more context on classification success. The kappa statistic of the OBIA was 0.75 which points to a substantial agreement between the ground truth NAIP imagery and the OBIA classification result. However, given the difference between the kappa statistic and overall accuracy values as well as the disparity in classification accuracy values between land cover classes, further context is necessary to determine classification success.

Table 7. OBIA accuracy assessment confusion matrix

	Tree	Not Tree	Total	User Accuracy
Tree	88	12	100	88.0%
Not Tree	41	1359	1400	97.1%
Total	129	1371	1500	N/A
Producer Accuracy	68.6%	99.1%	N/A	Overall Accuracy: 75.6%

4.3 Deep Learning Classification

The result of the deep learning classification was a 60-centimeter spatial resolution raster image of the study area which is classified into 'tree' and 'not tree' land cover classes. As seen in Figure 19, the 'tree' land cover class was colored in HEX#38A800 whilst the 'not tree' areas are left transparent. Using the 'Extract by Attribute' tool, the number of raster pixels in the 'tree' land cover class was identified and divided by the total number of pixels in the study area to determine percent area of tree canopy. It was determined that the deep learning classification identified 1.8% of the image scene as tree canopy, or 0.13 square miles.
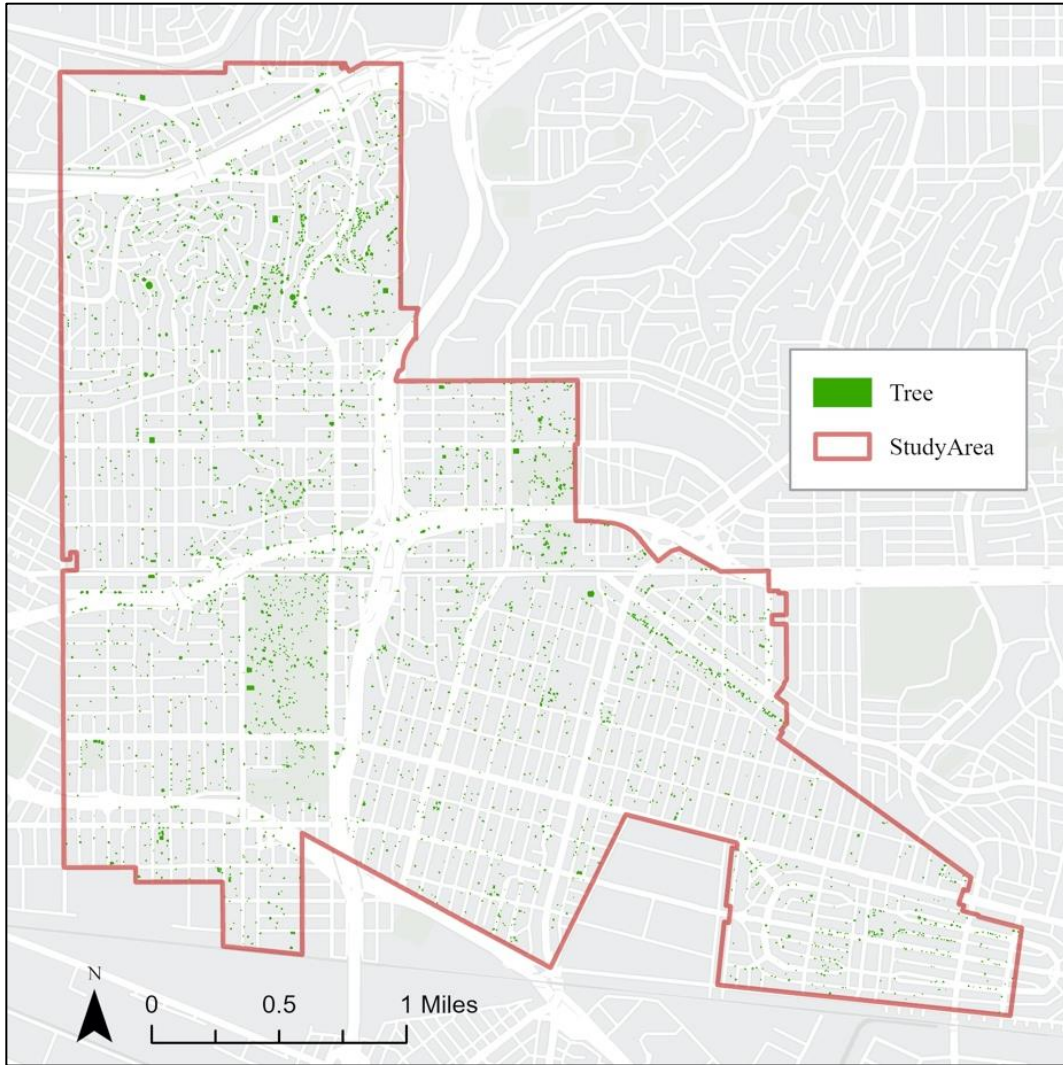
Figure 19. Deep learning tree canopy classification

According to the accuracy assessment of the deep learning classification of tree canopy, overall classification accuracy was 94.5%. This suggests a successful classification given a classification accuracy result substantially greater than 90%. However, like the accuracy assessment result of both the PBIA and OBIA, this is challenged by significant disparity in the producer accuracy between the 'tree' and 'not tree' land cover.

According to Table 8, the user accuracy of the classification of the 'tree' land cover class was 80.0%. This is a result of the low rate of false positive classifications as 20 of the 100

accuracy assessment points which were misidentified as 'tree' in the deep learning classified image instead belonged to the 'not tree' class according to the ground truth NAIP imagery. In contrast, the user accuracy of the 'not tree' land cover class was 97.1%. given only 62 of the 1400 accuracy assessment points were misclassified as 'not tree' according to the OBIA image and instead belong to the 'tree' class according to ground truth imagery. However, the disparity in the percent producer accuracy of classification between 'tree' and 'not tree' classes is greater than the disparity in user accuracies. The producer accuracy of the 'tree' land cover class was 56.6% due to the extreme rate of false negative classifications. Of the 142 accuracy assessment points which belong to the 'tree' class according to the ground truth NAIP imagery, 62 of which were misclassified as 'not tree' in the deep learning classification. This is contrasted by a 98.5% producer accuracy of the 'not tree' class given only 12 false 'tree' classifications in the deep learning result relative to the ground truth imagery.

Given the difference in classification accuracy per land cover class, the kappa statistic of this classification assessment can be used to provide more context on classification success. The kappa statistic of the OBIA was 0.63 which suggests only moderate to substantial agreement between the ground truth NAIP imagery and the OBIA classification result. Given this disparity between the kappa statistic and overall accuracy values as well as the disparity in classification accuracies per land cover class, further context is necessary in defining classification success.

Table 8. Deep learning accuracy assessment confusion matrix

	Tree	Not Tree	Total	User Accuracy
Tree	80	20	100	80.0%
Not Tree	62	1338	1400	95.6%
Total	142	1358	1500	N/A
Producer Accuracy	56.6%	98.5%	N/A	Overall Accuracy: 63.2%

4.4 Data Fusion Classification

The result of the data fusion classification was a 60-centimeter spatial resolution raster image of the study area which is classified into 'tree' and 'not tree' land cover classes. As seen in Figure 20, the 'tree' land cover class was colored in HEX#38A800 whilst the 'not tree' areas are left transparent. Using the 'Extract by Attribute' tool, the number of raster pixels in the 'tree' land cover class was identified and divided by the total number of pixels in the study area to determine percent area of tree canopy. Then, by dividing the count of tree canopy pixels by the total number of pixels in the study area it was determined that the pixel-based classification of tree canopy identified 8.3% of the image scene as tree canopy, or 0.62 square miles.
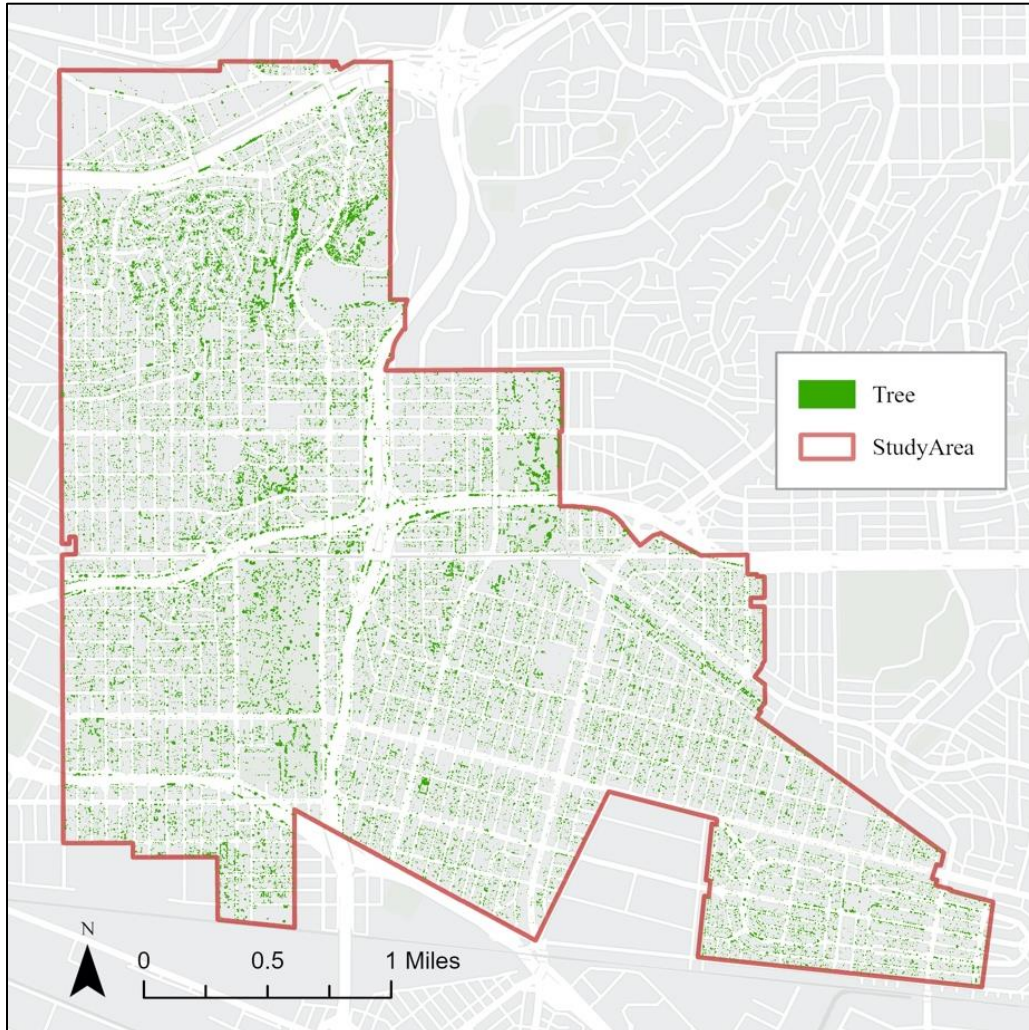
Figure 20. Data fusion tree canopy classification

According to the accuracy assessment of the data fusion classification of tree canopy, overall classification accuracy was 98.9%, the highest of all four classification types which suggests a successful classification given a classification accuracy result greater than 90%. Furthermore, the similarity of user and producer accuracy between land cover classes suggests more consistent classification performance.

According to Table 9, user accuracy of the classification of the 'tree' land cover class was 92.0%. This is given the low rate of false positive classifications as only eight of the 100

accuracy assessment points which belong to the 'tree' class according to the ground truth NAIP imagery were misidentified as 'not tree' according to the data fusion output. Similarly, the user accuracy of the 'not tree' land cover class was 99.5%. This is given that only six of the 1,150 accuracy assessment points classified as 'not tree' according to the ground truth NAIP were misclassified as 'tree' in the data fusion output. However, the disparity in the percent producer accuracy of classification between 'tree' and 'not tree' classes is greater than the disparity in user accuracies. The producer accuracy of the 'tree' land cover class was 68.6% due to the high rate of false negative classifications. Of the 129 accuracy assessment points which belong to the 'tree' class, according to the ground truth NAIP imagery, 41 of which were misclassified as 'not tree' in the data fusion classification. This is contrasted by a 99.1% producer accuracy of the 'not tree' class given only 12 false 'tree' classifications in the OBIA result relative to the ground truth imagery.

Given the difference in classification accuracy per land cover class, the kappa statistic of this classification assessment was used to provide more context on classification success. The kappa statistic of the data fusion classification was 0.92 which suggests near perfect agreement between the ground truth NAIP imagery and the data fusion result. Furthermore, given the minimal difference between the kappa statistic and overall accuracy values returned by this analysis' accuracy assessment the data fusion classification of tree canopy can be deemed successful.

Table 9. Data fusion accuracy assessment confusion matrix

	Tree	Not Tree	Total	User Accuracy
Tree	92	8	100	92.0%
Not Tree	6	1144	1150	99.5%
Total	98	1152	1250	N/A
Producer Accuracy	93.9%	99.3%	N/A	Overall Accuracy: 98.9%

Chapter 5 Discussion

Based on the results of the accuracy assessment of each image classification process, the data fusion classification methodology was identified as the optimal image classification type. The data fusion classification produced the most consistent classification output given its high classification accuracy of both the 'tree' and 'not tree' class. Despite its marginally longer geoprocessing times, the stepwise nature of data fusion methodology allows for customization in future iterations despite requiring a more robust reclassification process. Future image classification iterations may look to incorporate LiDAR derivatives in canopy edge feature classification whilst leveraging NDVI to fill tree objects to avoid complications of pixel shift and mixing. Future analyses may look to automate a data fusion classification using deep learning to capitalize on the benefits of both classification types. Ultimately, the findings of this analysis lay the groundwork to develop more robust tree management datasets for Los Angeles's future TPI efforts which can be later leveraged to quantify the impact of the UTC on heat and air quality.

5.1 Findings

This thesis aimed to compare four different image classification methodologies in their ability to accurately identify tree canopy from satellite imagery of Los Angeles in a replicable manner. Thus, the classifications were compared according to both the accuracy of the results and the complexity of processing. Based on the processing time information collected in both ArcGIS Pro and eCognition during the analysis, the decision on the most suitable classification method according to geoprocessing load was made.

The PBIA was completed in approximately four to five hours of total analysis time split between pre-processing, sample data collection, and tool geoprocessing. The pre-processing

steps of data collection, imagery projection, and masking of its spatial extent to the study area were completed in one hour, however, this was negligible given this was repeated across all classification methodologies. Sample data collection of all 700 training data sample pixels across the seven desired land cover classes was completed in approximately three to four hours. The sample data collection time for other iterations of this same PBIA analysis may fluctuate given the variety of factors which influence processing difficulty. For example, a study area with a greater variety in land use typologies would result in a more complex set of built environment conditions which would increase the spectral complexity of the image pixels. This could necessitate an increase in land cover classes in the final classification to capture all built environment conditions in the image as well as an increase in the number of sample pixels per class to ensure the entire spectral range of each land cover class is captured. This resulted in a marginally successful overall classification accuracy of 72.3% that was impacted by low classification accuracy of the 'tree' land cover class; however, this is expected given the PBIA classification's function as an analytical control.

The OBIA classification was intended to create an output result more accurate than that of the PBIA with a marginal increase in geoprocessing time and complexity. Given the PBIA and OBIA share input data, pre-processing was ignored from total processing time as in the PBIA. Segmentation of the input NAIP imagery for this analysis took approximately one to two hours given it required iteration to identify the ideal segmentation parameter values. Additionally, given the positive relationship larger raster file sizes and geoprocessing times in ArcGIS Pro, any future iterations of this OBIA which use larger raster data will suffer from a scaled increase in geoprocessing. Next, OBIA training data collection was completed in approximately six hours, an increase relative to that of the PBIA given the increase in sample data complexity. Whilst

PBIA training data only captures individual pixels in the image scene which represent each land cover class, OBIA training data captures user-drawn polygon shapes which intersect with all image objects that feature the spectral and spatial characteristics of the desired land cover class. Thus, any increases in the spectral and spatial complexity of the image used in classification may result in increases to total analysis time relative to that of the PBIA given the added complexity of training data collection. Unfortunately, the OBIA classification resulted in a 75.6% overall classification accuracy, only a negligible improvement over the PBIA despite nearly double the processing time. Additionally, the OBIA produced a more inconsistent classification given the user accuracy of the 'tree' class in the OBIA is 14.4% more accurate than the PBIA whilst the producer accuracy of the same 'tree' class in the OBIA is 7.1% less accurate than the PBIA. Thus, the OBIA cannot be identified as a decidedly more successful than the control PBIA.

The deep learning 'Tree Segmentation' classifier used in ArcGIS Pro for this analysis was used to compare the ability of deep learning classifiers in producing similarly accurate results relative to traditional PBIA and OBIA classifiers at a fraction of the total processing time and load. The pre-processing of the deep learning classification, primarily dedicated to extracting three-band imagery out of the original four-band NAIP image, took approximately 30 minutes to complete given the run time of the 'extract bands' tool. Next, processing of the image via the 'tree classification' classifier was completed in approximately 5.5 hours. Processing time was exclusively dedicated to the running of the deep learning classifier given it does not require any training data sampling to assist. Thus, the simplicity of the classifier justifies its use given the ease of replicability, however, its processing times may be subject to change with differences in the size of the input imagery data and differences in the processing capability of the workstation used for analysis.

Given the processing simplicity of deep learning classifiers and the impact data size has on analytical complexity, this thesis suggests the automation of this classification type. For example, Gamanya, Maeyer, and Dapper (2009) suggest the automation of LANDSAT and ASTER imagery across a single study area into the Department of Food and Agriculture's Land Cover system. Gamanya, Maeyer, and Dapper (2009) automate their classification system to classify multiple sets of input imagery within the same study area extent. Future iterations of the deep learning classification proposed in this thesis which attempt to classify across a larger study area may look to automate classification across multiple smaller study area segments so to ensure digestibility without the need for manually conducting classification on each segment. That said, use of deep learning classifiers in ArcGIS Pro requires the installation of the 'Deep Learning Libraries' extension which requires an NVIDIA GPU with CUDA Compute Capability 6.1 or later, NVIDIA GPU drivers version 527.1 or higher, and 8 gigabytes of dedicated graphics memory. Additionally, different deep learning classifiers feature different hardware compatibility requirements which exacerbate the issue of replicability and feasibility. Ultimately, given the 63.2% overall classification accuracy of the 'tree segmentation' deep learning classification result the classifier was deemed inadequate despite its ease of use.

Finally, the data fusion image classification analysis conducted in eCognition produced the classification result with ideal output accuracy yet was limited by analytic load and complexity. Geoprocessing was divided into pre-processing and ruleset development. Pre-processing was comprised of sourcing and merging LiDAR data into a singular dataset which covered the study area extent and the extraction of derivative products, like an nDSM. LiDAR sourcing and merging took approximately two hours to complete with 30 minutes being allocated to data sourcing. The remaining one hour and 30 minutes of processing was dedicated to

converting the raw LiDAR data into ArcGIS Pro compatible .lasd data type. Next, the creation of all LiDAR derivative raster datasets using the 'LAS to Raster' tool was completed in one hour of processing time per dataset. The processing time required to derive these raster datasets, however, is susceptible to change depending on the size and complexity of input data. For example, the pre-processing time of any analysis iterations completed on a larger study area extent would compound due to the larger file sizes requiring an increased number of analysis steps and increased geoprocessing time.

Ruleset development was completed in an iterative process. Although extensive literature on data fusion analysis in eCognition already outlines the tools necessary to complete the analysis, user-defined iteration is necessary given each rule set is developed based on values hosted in the input raster data. Rule set development was completed in approximately 12 hours, however, future iterations of this analysis which look to develop a more rigorous classification should expect longer rule development time. Once the classification rule set was developed, classification geoprocessing was completed in eCognition in 10 minutes. Thus, future data fusion classification methodologies should note analysis time must be dedicated to manual classification development. Based on these results, it was concluded that the data fusion image classification methodology is the best classification method given its high output accuracy and short processing times relative to the size of the study area and data sets used for analysis.

5.2 Error and Implications

This chapter discusses the various reasons for error in this analysis and how they implicate the adequacy of the result. The PBIA struggled in differentiating the 'tree' class from the 'shrub/grass' land cover class due to the spectral similarity of the training data pixels used for analysis. The OBIA similarly struggled in separating the 'tree' class from other natural land

cover classes specifically in instances of proximity given the object-based model's prioritization of spatial, geometric, and spectral similarity. Despite its ease of replicability, the deep learning classification produced inadequate accuracy results given its one step pretraining on natural forest tree imagery incongruent with the characteristics of the urban study area. The data fusion classification produced the most accurate result, however, at times misclassifies tree canopy given temporal discrepancies in the collection time of input data. Future practitioners who look to employ a similar data fusion classification must ensure a like temporal resolution across all datasets to maintain classification adequacy.

5.2.1 PBIA

The PBIA conducted for this thesis failed to adequately classify UTC due to a difficulty differentiating tree canopy pixels from vegetation with like spectral qualities. The accuracy assessment results of the PBIA indicate an unsuccessful classification of the 'tree' land cover class given the insufficient user and producer accuracies of the 'tree' land cover class: 73.6% and 75.7% respectively. Based on a visual inspection of the result on a larger scale shown in Figure 21, the PBIA struggled most with differentiating the 'tree' class from the 'grass/shrub' class in the initial seven-class schema. The PBIA both misclassified 'tree' class for the 'grass/shrub' class and misclassified the 'grass/shrub' class as the 'tree' class. This is likely due to overlap in the spectral characteristics of the training pixels used to train both the 'tree' and 'shrub/grass' land cover classes.

Figure 21. PBIA misclassified grass pixels

According to Shackelford and Davis (2003), PBIA classifiers decide the land cover class

of each pixel by comparing the spectral values of each individual pixel in an image against the

spectral values of the training data collected for classification. Thus, any spectral overlap in the

training data collected per class could cause confusion and misclassification between like

classes. For example, both vegetation pixels identified in the 'grass/shrub' class, like lawns or

fields, and 'tree' class pixels share similar green and yellow pixels which could be identified as

tree or grass pixels dependent on their specific reflectance value. The misclassification error of

the PBIA between the 'tree' and 'grass/shrub' class is expressed in the result given that these two

classes are later reclassified into to the 'tree' and 'not tree' class. Other land cover classes which share spectral qualities, like the 'paved ground' and 'building' class are also susceptible to similar misclassification, however, this is corrected for later when the seven-class scheme is reclassified into a two-class scheme, merging these similar field into the same class. This error, however, is not corrected for between the 'tree' and 'not tree' classes given that they remain separate and are not reclassified into the same land cover class. The PBIA used the SVM classifier which performs better in instances of limited training data, however, still struggles when differentiating homogeneous land cover classes.

5.2.2 OBIA

Like the PBIA, the OBIA classification conducted in this thesis also failed to adequately classify the 'tree' land cover class due to a difficulty separating the tree objects from like vegetation objects in the study area. The 75.6% overall classification accuracy of the analysis is explained by the discrepancy in the classification accuracy of the two identified land cover classes in which the user and producer accuracies of the 'tree' land cover class of interest are between 10% and 20% less accurate than that of the 'not tree' land cover class. A visual inspection of the result of the seven-class OBIA revealed a difficulty in differentiating the 'tree' from the 'shrub/grass' class, specifically in instances in which 'tree' and 'shrub/grass' object boundaries overlap like in lawns on private property.

Object-based image classification classify groups of image pixels into homogeneous, contiguous image objects based on spectral similarity, spatial proximity, and geometric similarity (Shackelford and Davis 2003). In sample data collection, all image objects with pixels that belong to the classification object of desire in the image scene, like tree pixels, are to be selected. Training data samples must capture both the geometry and spectral specificity of objects in land

cover class. Error in which adjacent 'tree' objects are misclassified 'grass/shrub' objects was likely caused by the selection of sample objects which share the spectrally similar pixels belonging to opposite land cover classes. As seen in Figure 22, these objects often lie along the boundary of a given feature and overlap into boundary of an adjacent feature, like the edge of a tree canopy in the image scene. To solve for this error, one must reiterate upon the segmentation process to produce smaller segmented objects which adhere more explicitly to the geometry of their respective land cover class feature. Thus, future iterations of a similar OBIA may look to employ more stringent segmentation parameters resulting in the creation of smaller, more homogeneous image objects with less overlap across land cover classes.

Figure 22. OBIA result tree canopy and grass objects overlap

5.2.3 Deep Learning

Due to the resolution of the NAIP imagery used in this analysis and one-step training used to train the deep learning classifier, the deep learning classification of tree canopy failed to capture ample street and private tree cover. The classifier used for analysis was the 'Tree Canopy' deep learning package provided in the ArcGIS Living Atlas data catalog. This package uses the Segment Anything Model (SAM) developed by Meta AI for accurate image segmentation with limited or no training data. Despite superior performance when segmenting geometrically defined objects like trees or buildings according to Osco et al. (2023), the deep learning classification conducted in this thesis produced an inadequate 63.2% overall classification accuracy. This is likely because the ArcGIS Tree Segmentation deep learning package provided in the catalog uses a one-shot approach trained on imagery from the National Ecological Observatory Network. Given that this training data likely does not share the spectral or spatial characteristics of the tree features of the study area, this discrepancy is likely the reason for poor performance. The resultant classification specifically failed to capture smaller trees or trees with non-dense canopy, as seen in Figure 23, likely because the deep learning model is trained on a true forest representation of tree canopy. Additionally, the SAM model struggled to achieve maximum classification performance when used on imagery with a larger than 30-centimeter resolution, like the 60-centimeter resolution NAIP imagery used for this thesis (Osco et al. 2023). Future analyses may look to employ the SAM model separately to leverage its no step processing capabilities or train the SAM model into a custom one step process.

Figure 23. Deep learning classification tree canopy and grass objects overlap

5.2.4 Data Fusion

Despite a temporal disparity in the collection times of all input data used in the analysis,

the data fusion classification produced the most accurate and actionable result. However, the

NDVI used in the analysis produced error in both misclassified tree canopy edge pixels and

whole misclassified tree objects within the scene. First, given the one-year temporal disparity in

the capture times of the NAIP four-band imagery and the LARIAC LiDAR point cloud,

classification using the NDVI data derived from the NAIP imagery results in the addition of trees

in the final classification. The NDVI dataset was incorporated in the second half of the rule set

classification thus accounting for trees which existed in the NDVI image and not in the original

LiDAR imagery, as seen in Figure 19. Despite this error, future iterations should maintain

incorporating NDVI later in their data fusion classification given canopy detection error inherent

to NDVI capture. According to Towers (2021), the existence of shade in an image scene due to

high illumination angles falsely adjusts reflectance values along tree canopy edges. Thus, NDVI

must remain incorporated later in the data fusion classification. Regardless, this error effect can

still be observed at the edge of certain tree canopy objects, as seen in Figure 24, resulting in

misshapen tree shapes. Future iterations of this data fusion analysis should instead look to

incorporate NDVI classification for internal tree canopy objects while leveraging LiDAR to

classify tree canopy borders.

Figure 24. Nonexistent tree polygons in data fusion result

5.3 Future TPI Development

This thesis conducted a comparison of four different classification methods in their ability to identify the existence of tree canopy in satellite imagery of Los Angeles. The result was a quantification of the area of tree canopy across the study area per image classification type. Although useful for comparison, this result is not actionable in urban forestry given a lack of description on tree characteristics, like canopy shape, tree age, and tree health. Instead, future iterations of this data fusion analysis may look to incorporate further LiDAR surface data into an identification of more specific tree characteristics for the sake of urban tree management.

For example, Zhong et al. (2022) utilized UAV hyperspectral imagery and LiDAR point cloud data in an identification of both tree heights and tree species in the forests of northeast China. Zhong et al. (2022) segment the LiDAR point cloud into individual tree point locations which is uniquely useful in identifying tree positions hidden by the canopy top cover in satellite imagery. This analysis is especially useful in identifying the extent of tree planting on private property on which the City of Los Angeles is unable to track planting progress. Additionally, Wang et al. (2023) propose an analysis which estimates forest canopy heights in a canopy height model according to similar LiDAR point cloud data. Both tree height ranges and tree species information are already collected in the City of Los Angeles's current street tree inventory, however, this can only be managed in the public right-of-way. Thus, the city is left with little information on current planting conditions on private property. Future analysis iterations which incorporate the identification of tree heights and species in their classification of the UTC can identify the crucial information necessary to manage tree planting on private land thus supporting the city's goal to develop an 'Adopt-a-Canopy' residential planting operation as outlined in the Green New Deal.

Whilst the result of this thesis provides opportunity to develop and compare the City of Los Angeles's current planting conditions against past approaches, they also allow for the future quantification of the impacts of Los Angeles's current Green New Deal. Given its young lifespan thus far, practitioners have been unable to conduct robust assessments on the success or impact of the tree planting goals outlined. In past comparisons, practitioners have estimated the potential success of TPIs in Los Angeles by comparing proposed tree planting goals against the space available and necessary to achieve them. For example, McPherson et al. (2008) estimates the potential Los Angeles's old 1-Million Trees planting initiative by counting and comparing the number potential tree planting sites in Los Angeles against the number of trees called for in the initiative. Given this analysis was conducted at the onset of the 1-Million Trees initiative, it acts as a predictor of success rather than a quantification. Thus, the existence of the Green New Deal provides an analytical opportunity to compare the approach of both the Green New Deal and 1-Million Trees TPIs as a judgement of success and efficacy. Furthermore, given the Green New Deal's standing as a long-range plan, this comparison may provide important context necessary to consider a restructuring of the plan.

The tree canopy area results quantified in this thesis set the groundwork for a quantification of tree canopy impact on physical health. Historically, research on the heating impacts of shade has prioritized the identification of the explanatory variables which define thermal impact (Spagnolo and Dear 2003). By identifying both the climatic and human factors which drive changes in heat, practitioners can model the magnitude each variable necessary to create a change in perceived heat. Furthermore, given the relationship between shade and heat impacts, practitioners, like Middel et al. (2016), can quantify the relationship the area of shade cover has on changes in temperature through regression-based modeling analyses. In the summer

of 2024, the LARIAC Consortium will release their LARIAC 7 LiDAR point cloud data which will significantly improve on the data's spatial resolution in comparison to LARIAC LiDAR data of past. A reiteration of the analytical methods proposed in this thesis using the 2024 LiDAR data would provide practitioners with a second time step necessary to quantify areal tree canopy growth over time.

Given the temporal resolution of each LARIAC collection corresponds with each development checkpoint outlined in the Green New Deal, the results of this analysis become a means of determining its success throughout its implementation. A time-stepped assessment of the Green New Deal would provide the opportunity to restructure the planting initiative to better achieve its goals. This, however, requires high-resolution, at least 1-meter spatial resolution, raster imagery of tree canopy cover. Whilst the methods of this thesis were able to achieve this result, its replicability is slow and limited. Thus, to standardize time stepped comparisons of success in TPIs, practitioners should improve upon deep learning and automated data fusion tree classification approaches to capitalize on their speed and reproducibility. As these methods become easier to reproduce, the repository of information gleaned by these results will become accessible. Furthermore, these results should be supplemented with data on local temperatures and air quality to determine how increased tree canopy affects these factors. Thus, rather than speculating on the perceived impacts of trees and their shade benefit, practitioners can use the results of this thesis to calculate the human impacts of trees down to the individual tree level. These results may be used to convince homeowners of the potential benefits of private tree planting or in the development of tree planting legislation as evidence to the importance and necessity of trees in the framework of current urban green infrastructure.

References

Agarwal, S., L.S. Vailshery, M. Jaganmohan, and N. Harini. 2013. "Mapping Urban Tree Species Using Very High Resolution Satellite Imagery: Comparing Pixel-Based and Object-Based Approaches," *ISPRS International Journal of Geo-Information* 2, no. 1: 236. https://doi.org/10.3390/ijgi2010220.

Eisenman, T.S., T. Flanders, R.W. Harper, R.J. Hauer, and K. Lieberknecht. 2021. "Traits of a Bloom: A Nationwide Survey of U.S. Urban Tree Planting Initiatives (TPIs)," *Urban Forestry & Urban Greening* 61, no. 61: 127006. https://doi.org/10.1016/j.ufug.2021.127006.

Gamanya, R., P.D. Maeyer, and M.D. Dapper. 2009. "Object-Oriented Change Detection for the City of Harare, Zimbabwe," *Expert Systems with Applications* 36, no. 1: 571–88. https://doi.org/10.1016/j.eswa.2007.09.067.

Gillespie, T.W., S. Pincetl, S. Brossard, J. Smith, S. Saatchi, D. Pataki, and J.D. Saphores. 2012. "A Time Series of Urban Forestry in Los Angeles," *Urban Ecosystems* 15, no. 1: 233–46. https://doi.org/10.1007/s11252-011-0183-6.

Han, L., W. Zhou, and W. Li. 2016. "Fine Particulate (PM2.5) Dynamics during Rapid Urbanization in Beijing, 1973–2013," *Scientific Reports* 6, no. 1: 23604. https://doi.org/10.1038/srep23604.

Hassler, B., B.C. McDonald, G.J. Frost, A. Borbon, D.C. Carslaw, K. Civerolo, and C. Granier. 2016. "Analysis of Long-Term Observations of NOx and CO in Megacities and Application to Constraining Emissions Inventories," *Geophysical Research Letters* 43, no. 18: 9920–30. https://doi.org/10.1002/2016GL069894

LeCun, Y., Y. Bengio, and G. Hinton. 2015. "Deep Learning," *Nature* 521, no. 7553: 436–44. https://doi.org/10.1038/nature14539.

Liu, D., and F. Xiao. 2010. "Assessing Object-Based Classification: Advantages and Limitations," *Remote Sensing Letters* 1, no. 4: 187–94. https://doi.org/10.1080/01431161003743173.

Liu, G.R., C.K. Liang, T.H. Kuo, T.H. Lin, and S.J. Huang. 2004. "Comparison of the NDVI, ARVI and AFRI Vegetation Index, Along with Their Relations with the AOD Using SPOT 4 Vegetation Data," *Terrestrial Atmospheric and Oceanic Sciences* 15, no. 15: 015. https://api.semanticscholar.org/CorpusID:52251994.

Lundqvist, J., P. Appasamy, and P. Nelliyat. 2003. "Dimensions and Approaches for Third World City Water Security," *Philosophical Transactions of the Royal Society of London* 358, no. 1440: 1985–96. https://doi.org/10.1098/rstb.2003.1382.

Ma, L., Y. Liu, X. Zhang, Y. Ye, G. Yin, and B.A. Johnson. 2019. "Deep Learning in Remote Sensing Applications: A Meta-Analysis and Review," *ISPRS Journal of Photogrammetry and Remote Sensing* 152, no. 152: 166–77. https://doi.org/10.1016/j.isprsjprs.2019.04.015.

McDonald, R., P. Green, D. Balk, B. Fekete, C. Revenga, M. Todd, and M. Montgomery. 2011. "Urban Growth, Climate Change, and Freshwater Availability," *Proceedings of the National Academy of Sciences of the United States of America* 108, no. 108: 6312–17. https://doi.org/10.1073/pnas.1011615108.

McHugh, M.L. 2012. "Interrater Reliability: The Kappa Statistic," *Biochemia Medica* 22, no. 3: 276–82.

McPherson, G.E., J.R. Simpson, Q. Xiao, and W. Chunxia. 2008. "Los Angeles 1-Million Tree Canopy Cover Assessment." U.S. Department of Agriculture, Forest Service, Pacific Southwest Research Station. https://doi.org/10.2737/psw-gtr-207.

Middel, A., N. Selover, B. Hagen, and N. Chhetri. 2016. "Impact of Shade on Outdoor Thermal Comfort-a Seasonal Field Study in Tempe, Arizona," *International Journal of Biometeorology* 60, no. 12: 1849–61. https://doi.org/10.1007/s00484-016-1172-5.

O'Neil-Dunne, J., S. MacFaden, and A. Royar. 2014. "A Versatile, Production-Oriented Approach to High-Resolution Tree-Canopy Mapping in Urban and Suburban Landscapes Using GEOBIA and Data Fusion," *Remote Sensing* 6, no. 12: 12865. https://doi.org/10.3390/rs61212837.

O'Neil-Dunne, J.P., S.W. MacFaden, A. Royar, and K.C. Pelletier. 2013. "An Object-Based System for LiDAR Data Fusion and Feature Extraction," *Geocarto International* 28, no. 3: 227–42. https://doi.org/10.1080/10106049.2012.689015.

Osco, L.P., Q. Wu, E. Lopes de Lemos, W.N. Gonçalves, A.P.M. Ramos, J. Li, and J. Marcato. 2023. "The Segment Anything Model (SAM) for Remote Sensing Applications: From Zero to One Shot," *International Journal of Applied Earth Observation and Geoinformation* 124, no. 124: 103540. https://doi.org/10.1016/j.jag.2023.103540.

Ouma, Y.O., and R. Tateishi. 2014. "Urban Flood Vulnerability and Risk Mapping Using Integrated Multi-Parametric AHP and GIS: Methodological Overview and Case Study Assessment," *Water* 6, no. 6: 1515–45. https://doi.org/10.3390/w6061515.

Pincetl, S., T. Gillespie, D.E. Pataki, S. Saatchi, and J.D. Saphores. 2013. "Urban Tree Planting Programs, Function or Fashion? Los Angeles and Urban Tree Planting Campaigns," *GeoJournal* 78, no. 3: 475–93. https://doi.org/10.1007/s10708-012-9446-x.

Riley, C.B., and M.M. Gardiner. 2020. "Examining the Distributional Equity of Urban Tree Canopy Cover and Ecosystem Services across United States Cities," *PLoS One* 15, no. 2: e0228499. https://doi.org/10.1371/journal.pone.0228499.

Roman, L.A., L.A. Walker, C.M. Martineau, D.J. Muffly, S.A. MacQueen, and W. Harris 2015. "Stewardship Matters: Case Studies in Establishment Success of Urban Trees," *Urban Forestry & Urban Greening* 14, no. 4: 1174–82. https://doi.org/10.1016/j.ufug.2015.11.001.

Roy, S., J. Byrne, and C. Pickering. 2012. "A Systematic Quantitative Review of Urban Tree Benefits, Costs, and Assessment Methods across Cities in Different Climatic Zones," *Urban Forestry & Urban Greening* 11, no. 4: 351–63. https://doi.org/10.1016/j.ufug.2012.06.006.

Shackelford, A., and C.H. Davis. 2003. "A Combined Fuzzy Pixel-Based and Object-Based Approach for Classification of High-Resolution Multispectral Data over Urban Areas," *IEEE Transactions on Geoscience and Remote Sensing* 41, no. 41: 2354–63. https://doi.org/10.1109/TGRS.2003.815972.

Shahidan, M., and P. Jones. 2008. "Plant Canopy Planting Design in Modifying Urban Thermal Environment: Theory and Guidelines."

Shojanoori, R., and H. Shafri. 2016. "Review on the Use of Remote Sensing for Urban Forest Monitoring," *Arboriculture & Urban Forestry 42*, no. 42: 400–417. https://doi.org/10.48044/jauf.2016.034.

Sibaruddin, H.I., H.Z.M. Shafri, B. Pradhan, and N.A. Haron. 2018. "Comparison of Pixel-Based and Object-Based Image Classification Techniques in Extracting Information from UAV Imagery Data," *IOP Conference Series: Earth and Environmental Science* 169, no. 1: 012098. https://doi.org/10.1088/1755-1315/169/1/012098.

Spagnolo, J., and R.D. Dear. 2003. "A Field Study of Thermal Comfort in Outdoor and Semi-Outdoor Environments in Subtropical Sydney Australia," *Building and Environment* 38, no. 5: 721–38. https://doi.org/10.1016/S0360-1323(02)00209-3.

Spatari, S., Z. Yu, and F.A. Montalto. 2011. "Life Cycle Implications of Urban Green Infrastructure," *Environmental pollution (Barking, Essex : 1987)* 159, no. 8–9: 2174–79. https://doi.org/10.1016/j.envpol.2011.01.015.

Srinivasan, V., K.C. Seto., R. Emerson, and S.M. Gorelick. 2013. "The Impact of Urbanization on Water Vulnerability: A Coupled Human–Environment System Approach for Chennai, India," *Global Environmental Change* 23, no. 1: 229–39. https://doi.org/10.1016/j.gloenvcha.2012.10.002.

Sung, C.H. 2012. "Evaluating the Efficacy of a Local Tree Protection Policy Using LiDAR Remote Sensing Data," *Landscape and Urban Planning* 104, no. 1: 19–25. https://doi.org/10.1016/j.landurbplan.2011.09.009.

Towers, P.C., and C. Poblete-Echeverría. 2021. "Effect of the Illumination Angle on NDVI Data Composed of Mixed Surface Values Obtained over Vertical-Shoot-Positioned Vineyards," *Remote Sensing* 13, no. 5. https://doi.org/10.3390/rs13050855.

Wang, J., B. Huang, D. Fu, P.M. Atkinson, and X. Zhang. 2016. "Response of Urban Heat Island to Future Urban Expansion over the Beijing–Tianjin–Hebei Metropolitan Area," *Applied Geography* 70, no. 70: 26–36. https://doi.org/10.1016/j.apgeog.2016.02.010.

Wang, S., C. Liu, W. Li., S. Jia, and H. Yue. 2023. "Hybrid Model for Estimating Forest Canopy Heights Using Fused Multimodal Spaceborne LiDAR Data and Optical Imagery," *International Journal of Applied Earth Observation and Geoinformation* 122, no. 122: 103431. https://doi.org/10.1016/j.jag.2023.103431.

Watkins, S.H., S.K. Mincey, J. Vogt, and S.P. Sweeney. 2017. "Is Planting Equitable? An Examination of the Spatial Distribution of Nonprofit Urban Tree-Planting Programs by Canopy Cover, Income, Race, and Ethnicity," *Environment and Behavior* 49, no. 4: 452–82. https://doi.org/10.1177/0013916516636423.

Xiao, Q., and E.G. McPherson. 2002. "Rainfall Interception by Santa Monica's Municipal Urban Forest," *Urban Ecosystems* 6, no. 4: 291–302. https://doi.org/10.1023/B:UECO.0000004828.05143.67.

Xiong, Y., S. Huang, F. Chen, H. Ye, C. Wang, and C. Zhu. 2012. "The Impacts of Rapid Urbanization on the Thermal Environment: A Remote Sensing Study of Guangzhou, South China," *Remote Sensing* 4, no. 7: 2033–56. https://doi.org/10.3390/rs4072033.

Yao, W., and Y. Wei. 2013. "Detection of 3-D Individual Trees in Urban Areas by Combining Airborne LiDAR Data and Imagery," *IEEE Geoscience and Remote Sensing Letters* 10, no. 6: 1355–59. https://doi.org/10.1109/LGRS.2013.2241390.

Yu, P.S., S.T. Chen, and S.E. Chang. 2006. "Support Vector Regression for Real-Time Flood Stage Forecasting," *Journal of Hydrology* 328, no. 3: 704–16. https://doi.org/10.1016/j.jhydrol.2006.01.021.

Zhang, J. 2010. "Multi-Source Remote Sensing Data Fusion: Status and Trends," International *Journal of Image and Data Fusion* 1, no. 1: 5–24. https://doi.org/10.1080/19479830903561035.

Zhong, H., W. Lin, H. Liu, N. Ma, K.Liu, R. Cao, T. Wang, and Z. Ren. 2022. "Identification of Tree Species Based on the Fusion of UAV Hyperspectral Image and LiDAR Data in a Coniferous and Broad-Leaved Mixed Forest in Northeast China," *Frontiers in Plant Science* 13, no. 13 September: 964769. https://doi.org/10.3389/fpls.2022.964769.

Zhuang, Y., D. Xie, and X. Yu. 2023. "Urban Tree Canopy and Environmental Justice: Examining the Distributional Equity of Urban Tree Canopy in Guangzhou, China," *International Journal of Environmental Research and Public Health* 20, no. 5: 4050. https://doi.org/10.3390/ijerph20054050.